

1 Responses to reviewer #1

2

3 This study of airborne observations of halogenated VOCs (HVOCs) represents a valuable addition to the
4 knowledge of these compounds over the Southern Ocean, where few data exist. The study confirms the
5 current view that the main sources of CHBr₃ and CH₂Br₂ are biological, and that CH₃I has both
6 biological and non-biological sources. The authors have put forward a novel concept of using enrichment
7 ratios of HVOCs to O₂ to infer the contribution or otherwise of ocean biological sources, and propose a
8 new function to estimate non-biological emission fluxes of CH₃I. The dataset has been used to evaluate
9 the CAM-Chem HVOC emission scheme at high latitudes in the Southern Hemisphere. The take home
10 message/s from this evaluation are rather opaque – they could do with being put in context. E.g., do they
11 infer that fluxes from these regions are poorly known, or problems with the models mixing /convection
12 schemes special to these latitudes, or issues with photo-oxidation rates?. In terms of presentation, the
13 paper has a number of typographical and other errors, listed below, and needs a thorough reading (I doubt
14 I captured all of them). However overall, I think this manuscript presents sufficiently novel results to be
15 suitable for publication, once these matters have been attended to.

16 We appreciate the reviewer's time and comments. We have done our best to clarify the goals and
17 findings of this study. We argue that emissions of HVOCs over the Southern Ocean are poorly known
18 using mixing ratio comparisons with a global climate model and state of the art biogenic flux
19 parameterizations based on chl *a* that show persistent model biases. Thereafter, we seek to address this
20 problem by proposing new approaches to estimate regional HVOC fluxes using airborne observations.
21 We demonstrate two additional approaches for deriving HVOC flux estimates using airborne
22 observations, and model output. We hope that the reviewer finds our article suitable for publication
23 following these revisions.

24

25 L34-38 The regional enrichment ratios should be put in context here - there is no explanation as their
26 relevance.

27 We no longer report enrichment ratios in the abstract. We do however, attempt to explain the role of O₂-
28 HVOC enrichment ratios in inferring a biological flux of HVOCs. This passage now reads, "The first
29 approach takes advantage of the robust relationships that were found between airborne observations of O₂
30 and CHBr₃, CH₂Br₂, and CHClBr₂; we use these linear regressions with O₂ and modeled O₂ distributions
31 to infer a biological flux of HVOCs." L30-33.

32

33 L51- 52 "Indeed, HVOCs may be among the most important sources of inorganic bromine to the whole
34 atmosphere (Murphy et al., in review)." This is not conventional wisdom and thus quite a bold
35 statement. Are the authors confident that the Murphy et al paper will be published soon?

36 Murphy et al. (2019) has now been published and the citation has been revised. We have also moderated
37 the language to reflect that this statement challenges conventional wisdom. This passage L50-54 now
38 reads, "In the marine boundary layer and lower troposphere, sea salt is the main source of reactive
39 bromine (Finlayson-Pitts 1982, Simpson et al. 2019). Yet HVOCs may also be a more important source
40 of inorganic bromine to the whole atmosphere than previously thought, according to a recent study, which
41 indicates that sea salt is scarce and insufficient to control the bromine budget in the middle and upper
42 troposphere (Murphy et al., 2019)."

43

44 L61-64 The anthropogenic sources of CH₃Br have changed over time and now are dominated by
45 quarantine and pre-shipment (QPS) applications (not controlled by the Montreal Protocol). Please stick to
46 the most recent information from WMO 2018 (and update the reference).

47 Both the information and citation on anthropogenic sources of CH₃Br have been revised in L65-68: “CH₃I
48 is also formed through non-biological reactions in surface seawater, and CH₃Br is emitted as a result of
49 quarantine and pre-shipment activities, which are not regulated by the Montreal Protocol (e.g., Moore and
50 Zafiriou; 1994, WMO 2018).

51

52 L119- 130 The last paragraph of the introduction would benefit from an introduction to the concept of
53 enrichment ratios of HVOCs to O₂, which feature prominently in the abstract.

54 We have revised this passage in L122-139 to read, “In Section 3.1 and 3.2, we report new airborne
55 observations of CHBr₃, CH₂Br₂, CH₃I, CHClBr₂, CHBrCl₂, and CH₃Br from high latitudes in the Southern
56 Hemisphere, where data are scarce, and large-scale regional mixing ratio comparisons for HVOCs with
57 the community earth system model (CESM) atmospheric component with chemistry (CAM-Chem). In
58 section 3.4, we present two novel approaches to estimate regional fluxes of HVOCs for comparison with
59 global climate models’ parameterizations or climatologies. One approach uses correlations of HVOCs to
60 marine, oxygen (O₂) of marine origin, as measured by deviations in the ratio of O₂ to nitrogen (N₂)
61 ($\delta(O_2/N_2)$ see Sect. 2.1.2 and 3.1.2) to determine the importance of regional biological HVOC sources.
62 The robust correlations of CHBr₃ and CH₂Br₂ with $\delta(O_2/N_2)$ are indicative of a strong biological source.
63 Our first approach exploits the ratio of HVOCs to oxygen (O₂) determined from linear regressions (i.e. the
64 enrichment ratio), and the ocean flux of O₂ from CESM’s ocean component, to estimate the marine
65 biogenic flux of several HVOCs. The second approach relies on observed HVOC mixing ratios, the
66 Stochastic Time-Inverted Lagrangian Transport (STILT) particle dispersion model and geophysical
67 datasets (see Sect. 2.3 and 3.3). We assess contributions from previously hypothesized regional sources
68 for the Southern Ocean, and estimate HVOC fluxes based on regressions between upstream influences
69 and observed mixing ratios and distributions of remotely sensed data.”

70

71 L235-245 The fact that the polyhalogenated bromocarbons are likely co-emitted is not new – there are
72 numerous papers that show this, and the discussion could elaborate on those a bit more. What is also
73 missing from this paragraph is a discussion of macroalgal sources of these compounds, although this is
74 presumably not relevant for the Antarctic.

75 We have expanded the discussion of previous findings of co-emitted polyhalogenated bromocarbons and
76 cited several additional studies. This passage L390 - 401 now reads, “Previous studies have documented
77 co-located source regions of CHBr₃ and CH₂Br₂ in the Southern Ocean (e.g. Hughes et al., 2009;
78 Carpenter et al., 2000; Nightingale et al. 1995; Laturmus et al. 1996), and laboratory studies have
79 demonstrated that phytoplankton and their associated bacteria cultures, including a cold water diatom
80 isolated from coastal waters along the Antarctic Peninsula and common to the Southern Ocean, produce
81 both CHBr₃ and CH₂Br₂ (Hughes et al., 2013; Tokarczyk and Moore 1994, Sturges et al., 1993). The non-
82 linearity observed in ratios of these two gases at low CHBr₃ may reflect the different rates of their
83 production or loss in seawater, or possibly, the influence of air masses from distant, more productive low-
84 latitude source regions. Several studies have documented bacterially mediated loss of CH₂Br₂, but not

85 CHBr₃, and report distinct ratios of CH₂Br₂ to CHBr₃ in seawater during the growth and senescent phases
86 of a phytoplankton bloom (e.g. Carpenter et al. 2009, Hughes et al 2013). ”

87

88 L244-245 “For instance, Huges et al. (2013) also report distinct seawater slopes between CH₂Br₂ to
89 CHBr₃ , when chl a was increasing.” It is not clear what is meant by this. Please rephrase

90 This statement has been rephrased on L398, “Several studies have documented bacterially mediated loss
91 of CH₂Br₂, but not CHBr₃, and report distinct ratios of CH₂Br₂ to CHBr₃ in seawater during the growth
92 and senescent phases of a phytoplankton bloom (e.g. Carpenter et al. 2009, Hughes et al 2013).”

93

94 L361- 366 “In both regions, the model under predicts CH₃I above the MBL, which may indicate slower
95 observed photochemical loss than the model predicts.” Has this been found in other CAM-Chem studies –
96 e.g. is it a general result? If not, could a different source emission distribution (i.e. more homogeneous
97 source) explain these results?

98 We have revised the text to reflect that indeed this result has been found in other CAM-Chem studies, and
99 that the observed difference at high latitudes in the SH at ~10 km altitude may be due to the zonal
100 transport of air masses from lower latitudes, where differences in CH₃I in the UTLS have also been
101 observed. For instance, in Ordonez et al. (2012), Fig. 10 illustrates the consistent under prediction of the
102 observed CH₃I mixing ratios, and these authors attribute this discrepancy to the strength of convective
103 cells rapidly transporting air masses to the UTLS. This section L494-499 now reads as follows: “In both
104 regions, the model under predicts CH₃I in the upper troposphere and lower stratosphere (UTLS), likely
105 stemming from the poleward transport of lower latitude air masses, where CAM-Chem also exhibits a
106 negative bias. Mixing ratio comparisons with CAM-Chem over the tropics (see Ordonez et al. Figure 10)
107 depict similar or larger discrepancies, and have been attributed to stronger than anticipated convective
108 cells in the tropics.”

109

110 L555-L560 onwards. There is no mention in Moore and Zarifou 1994 nor Richter and Wallace 2004 as
111 far as I can see on the influence of iron availability – do the authors mean iodide availability?!

112 We have both fixed a typo and clarified the discussion on proposed non-biological chemical mechanisms
113 for CH₃I production in the ocean, which include the radical recombination reaction proposed by Moore
114 and Zarifou (1994), and the substitution reaction, requiring an oxidant such as iron III, proposed by
115 Williams et al. (2007). This passage L563-569 now reads, “This non-biological source, though not fully
116 understood, requires light, a humic like substance at the surface ocean supplying a carbon source and
117 methyl group, and reactive iodine (Moore and Zarifou 1994; Richter and Wallace 2004). Thus far, two
118 chemical mechanisms have been proposed for the non-biological production of methyl iodide, one – a
119 radical recombination of a methyl group and iodine involving UV photolysis (e.g. Moore and Zarifou
120 1994), and the second, a substitution reaction involving the reduction of an oxidant, such as iron III (e.g.
121 Williams et al. 2007).”

122

123 L1036 – Note that units should be pmol m⁻² hr⁻¹ (not m²). Please state whether the values given for the
124 observations are means or medians. It would be also be good to include their ranges.

125 We have corrected this typo on L1068. The units on Table 1 now read “ $\text{pmol m}^{-2} \text{hr}^{-1}$.”

126

127 Ln 82. atmopsheric Ln 213. “oppose” should be “opposed” Ln 213. “Huges” should be “Hughes” Ln 242
128 : “HOVCs” Ln 469. “Zafarou” should be “Zafariou” Ln 980. “includind” LN 1015. “fluxed”

129 L81, L253, L391, L518, L1171- Typos have been corrected to read, “Atmospheric,” “opposed,”
130 “HVOCs,” “Zafariou,” and “fluxes.” Other typos previously listed have been deleted from the text.

131

132

133

134 **Novel approaches to improve estimates of short-lived halocarbon emissions during summer**
135 **from the Southern Ocean using airborne observations**

136 **Elizabeth Asher¹, Rebecca S. Hornbrook¹, Britton B. Stephens¹, Doug Kinnison¹, Eric J. Morgan⁵, Ralph F.**
137 **Keeling⁵, Elliot L. Atlas⁶, Sue M. Schauffler¹, Simone Tilmes¹, Eric A. Kort², Martin S. Hoecker-Martínez³,**
138 **Matt C. Long¹, Jean-François Lamarque¹, Alfonso Saiz-Lopez^{4,1}, Kathryn McKain^{7,8}, Colm Sweeney⁸, Alan J.**
139 **Hills¹, and Eric C. Apel¹**

140 ¹ National Center for Atmospheric Research, Boulder, Colorado, USA

141 ² University of Michigan, Climate and Space Sciences and Engineering, Ann Arbor, Michigan, USA

142 ³ University of Redlands, Physics Department, Redlands, California, USA

143 ⁴ Department of Atmospheric Chemistry and Climate, Institute of Physical Chemistry Rocasolano, CSIC,
144 Madrid, Spain

145 ⁵ Scripps Institution of Oceanography, University of California, San Diego, California, USA

146 ⁶ University of Miami, Department of Atmospheric Sciences, Miami, Florida, USA

147 ⁷ Cooperative Institute for Research in Environmental Sciences, University of Colorado, Boulder,
148 Colorado, USA

149 ⁸ National Oceanic and Atmospheric Administration, Boulder, Colorado, USA

150

151

152 **Abstract.**

153 Fluxes of halogenated volatile organic compounds (HVOCs) over the Southern Ocean remain
154 poorly understood, and few atmospheric measurements exist to constrain modeled emissions of
155 these compounds. We present observations of CHBr_3 , CH_2Br_2 , CH_3I , CHClBr_2 , CHBrCl_2 , and
156 CH_3Br during the O_2/N_2 Ratio and CO_2 Airborne Southern Ocean (ORCAS) study and the 2nd
157 Atmospheric Tomography mission (ATom-2), in January and February of 2016 and 2017. Good
158 model-measurement correlations were obtained between these observations and simulations from
159 the Community Earth System Model (CESM) atmospheric component with chemistry (CAM-
160 Chem) for CHBr_3 , CH_2Br_2 , CH_3I , and CHClBr_2 but all showed significant differences in
161 model:measurement ratios. The model:measurement comparison for CH_3Br was satisfactory and
162 for CHBrCl_2 the low levels present precluded us from making a complete assessment.
163 Thereafter, we demonstrate two novel approaches to estimate HVOC fluxes; the first approach
164 takes advantage of the robust relationships that were found between airborne observations of O_2
165 and CHBr_3 , CH_2Br_2 , and CHClBr_2 ; we use these linear regressions with O_2 and modeled O_2
166 distributions to infer a biological flux of HVOCs. The second approach uses the Stochastic
167 Time-Inverted Lagrangian Transport (STILT) particle dispersion model to explore the
168 relationships between observed mixing ratios and the product of the upstream surface influence
169 and sea ice, chl *a*, absorption due to detritus, and downward shortwave radiation at the surface,
170 which in turn relate to various regional hypothesized sources of HVOCs such as marine
171 phytoplankton, phytoplankton in sea ice brines, and decomposing organic matter in surface
172 seawater. These relationships can help evaluate the likelihood of particular HVOC sources, and
173 in the case of statistically significant correlations, such as was found for CH_3I , may be used to
174 derive an estimated flux field. Our results are consistent with a biogenic regional source of
175 CHBr_3 , and both non-biological and biological sources of CH_3I over these regions.

176

177 **1 Introduction**

178 Emissions of halogenated volatile organic compounds (HVOCs) influence regional atmospheric
179 chemistry and global climate. Through the production of reactive halogen radicals at high
180 latitudes, HVOCs contribute to tropospheric and stratospheric ozone destruction, and alter the
181 sulfur, mercury, nitrogen oxide and hydrogen oxide cycles (e.g. Schroeder et al., 1998; Boucher
182 et al., 2003; Bloss et al., 2005; von Glasow and Crutzen; 2007; Saiz-Lopez et al., 2007; Obrist et
183 al., 2011; WMO, 2018). In the marine boundary layer and lower troposphere, sea salt is the main
184 source of reactive bromine (Finlayson-Pitts 1982, Simpson et al., 2015). Yet HVOCs may also
185 be a more important source of inorganic bromine to the whole atmosphere than previously
186 thought, according to a recent study, which indicates that sea salt is scarce and insufficient to
187 control the bromine budget in the middle and upper troposphere (Murphy et al., 2019).

188 Phytoplankton and macroalgae in the ocean are the main sources to the atmosphere of several
189 very short-lived bromocarbons, including bromoform (CHBr_3), dibromomethane (CH_2Br_2),
190 dibromochloromethane (CHClBr_2), and bromodichloromethane (CHBrCl_2) (Moore et al., 1996;
191 Carpenter et al. 2003; Butler et al., 2007; Raimund et al., 2011). Other HVOCs, such as methyl

Elizabeth Asher 7/5/2019 2:01 PM

Deleted: -side

Elizabeth Asher 7/5/2019 2:05 PM

Deleted: We show mixing ratio comparisons

Elizabeth Asher 7/6/2019 2:51 PM

Deleted: Thereafter, we

196 iodide (CH₃I), and methyl bromide (CH₃Br) have many natural sources, such as coastal
197 macroalgae, phytoplankton, temperate forest soil and litter, and biomass burning (e.g., Bell et al.,
198 2002; Sive et al., 2007; Colomb et al. 2008; Drewer et al., 2008). CH₃I is also formed through
199 non-biological reactions in surface seawater, and CH₃Br is emitted as a result of quarantine and
200 pre-shipment activities, which are not regulated by the Montreal Protocol (e.g., Moore and
201 Zafiriou; 1994, WMO 2018). Over the Southern Ocean specifically, hypothesized sources of
202 HVOCs include: coastal macroalgae, phytoplankton, sea ice algae, and photochemical or dust
203 stimulated non-biological production at the sea surface (e.g., Abrahamsson et al. 2018, Manley
204 and Dastoor 1998; Moore and Zafiriou 1994; Moore et al., 1996; Richter and Wallace 2004;
205 Williams et al., 2007; Tokarczyk and Moore 1994; Sturges et al., 1992).

206 We largely owe our current understanding of marine HVOC emissions over the Southern Ocean
207 to ship-based field campaigns and laboratory process studies (e.g., Abrahamsson et al. 2004a,b;
208 Atkinson et al., 2012; Carpenter et al., 2007; Moore et al., 1996; Chuck et al., 2005; Butler et al.,
209 2007; Raimund et al., 2011; Hughes et al., 2009; Mattsson et al. 2013; Hughes et al., 2013).

210 These studies have reported surface water and sea-ice HVOC supersaturation and corresponding
211 elevated levels of HVOCs in the marine boundary layer (MBL) in summer, and have identified
212 numerous biological and non-biological ocean sources for these compounds. Mattsson et al.
213 (2013) noted that the ocean also acts as a sink for HVOCs, when HVOC undersaturated surface
214 waters equilibrate with air masses transported from source regions. The spatially heterogeneous
215 ocean sources of CHBr₃ and CH₂Br₂ at high latitudes in the Southern Hemisphere, are often
216 underestimated in global atmospheric models (Hossaini et al., 2013; Ordoñez et al., 2012; Ziska
217 et al., 2013). Ship-based and Lagrangian float observations provide invaluable information on
218 the sources and temporal variability of compounds in the surface ocean. These methods offer the
219 advantage of simultaneous measurements of both air and seawater to evaluate the gases'
220 saturation state in the surface ocean and calculate fluxes. Yet ship-based measurements onboard
221 these slow moving platforms also have drawbacks: they under sample the spatial variability of
222 HVOCs (e.g., Butler et al., 2007) and require assumptions about gas-exchange rates to estimate
223 fluxes.

224 To disentangle the roles of atmospheric transport and spatial variability of emissions on HVOC
225 distributions requires large-scale atmospheric observations. At low latitudes, large-scale
226 convection at the intertropical convergence zone carries bromocarbons and other HVOCs into
227 the free troposphere and lower stratosphere (e.g., Liang et al., 2014; Navarro et al., 2015). Polar
228 regions are characterized by stable boundary layers in summer. Wind shear, frontal systems, and
229 internal gravity waves create turbulence and control vertical mixing within and across a stable
230 polar boundary layer (e.g. Anderson et al., 2008), and small, convective plumes may form over
231 the marginal sea ice zone, related to sea ice leads as well as winds from ice-covered to open-
232 ocean waters (e.g. Schnell et al., 1989). As a result of limited vertical transport in these regions,
233 however, air-sea fluxes lead to strong vertical gradients. Zonal transport from lower latitudes has
234 a large impact on the vertical gradients of trace gas mixing ratios over polar regions (Salawitch
235 2010). Given their extended photochemical lifetimes at high latitudes (see Sect. 2.3 for a brief
236 discussion), many HVOC distributions are particularly sensitive to zonal transport at altitude.

Elizabeth Asher 7/7/2019 9:48 AM

Deleted: the

Elizabeth Asher 7/7/2019 9:49 AM

Deleted: ,

239 Aircraft observations can rapidly map basin-wide vertical distributions, support quantitative flux
240 estimates, and provide spatial constraints to atmospheric models (e.g. Xiang et al., 2010;
241 Stephens et al., 2018; Wofsy et al., 2011). Few airborne observations of HVOCs exist at high
242 latitudes in the Southern Hemisphere. Two earlier aircraft campaigns that have measured
243 summertime HVOCs in this region are the first Aerosol Characterization Experiment (ACE-1;
244 Bates et al., 1999) and the first High-performance Instrumented Airborne Platform for
245 Environmental Research (HIAPER) Pole-to-Pole Observations (HIPPO; Wofsy, 2011)
246 campaign. For these two aircraft campaigns, whole air samples were collected onboard the
247 NSF/NCAR C-130 and the NSF/NCAR Gulfstream V (GV) during latitudinal transects over the
248 Pacific Ocean as far south as 60° S and 67° S, respectively. However, the ACE-1 and HIPPO
249 campaigns obtained relatively few whole air samples in this region, with ≤100 samples poleward
250 of 60° S combined (e.g., Blake et al., 1999; Hossaini et al., 2013). ACE-1 measurements of CH₃I
251 in the MBL indicate a strong ocean source between 40° S and 50° S in austral summer, with
252 mixing ratios above 1.2 pmol below ~1 km (Blake et al., 1999).

Elizabeth Asher 6/16/2019 4:20 PM

Deleted: air-sea

253 HVOC emissions are frequently incorporated into earth system models, using either
254 climatologies or parameterizations based on satellite observations of chlorophyll and
255 geographical region and evaluated using mixing ratio comparisons with airborne observations. In
256 Section 3.1 and 3.2, we report new airborne observations of CHBr₃, CH₂Br₂, CH₃I, CHClBr₂,
257 CHBrCl₂, and CH₃Br from high latitudes in the Southern Hemisphere, where data are scarce, and
258 large-scale regional mixing ratio comparisons for HVOCs with the community earth system
259 model (CESM) atmospheric component with chemistry (CAM-Chem). In section 3.4, we
260 present two novel approaches to estimate regional fluxes of HVOCs for comparison with global
261 climate models' parameterizations or climatologies. One approach uses correlations of HVOCs
262 to marine, oxygen (O₂) of marine origin, as measured by deviations in the ratio of O₂ to nitrogen
263 (N₂) (δ(O₂/N₂) see Sect. 2.1.2 and 3.1.2). We exploit robust ratios of HVOCs to oxygen (O₂)
264 determined from linear regressions (i.e. the enrichment ratio), and the ocean flux of O₂ from
265 CESM's ocean component, to estimate the marine biogenic flux of several HVOCs. The second
266 approach relies on observed HVOC mixing ratios, the Stochastic Time-Inverted Lagrangian
267 Transport (STILT) particle dispersion model and geophysical datasets (see Sect. 2.3 and 3.3).
268 We assess contributions from previously hypothesized regional sources for the Southern Ocean,
269 and estimate HVOC fluxes based on regressions between upstream influences and observed
270 mixing ratios and distributions of remotely sensed data.

Elizabeth Asher 7/7/2019 10:08 AM

Deleted: climate

272 **2 Methods**

273 **2.1 Measurements**

274 Atmospheric measurements for this study were collected at high latitudes in the Southern
275 Hemisphere as part of the O₂/N₂ Ratio and CO₂ Airborne Southern Ocean (ORCAS) study
276 (Stephens et al., 2018), and the second NASA Atmospheric Tomography Mission (ATom-2),
277 near Punta Arenas, Chile (Fig. 1). The ORCAS field campaign took place from Jan. 15 – Feb.
278 29, 2016 onboard the NSF/NCAR GV. On Feb. 10 and 13, 2017 the sixth and seventh ATom-2
279 research flights passed over the eastern Pacific sector poleward of 60° S (defined here as Region

Elizabeth Asher 7/5/2019 2:13 PM

Deleted: Observations

Elizabeth Asher 7/5/2019 2:13 PM

Deleted: Overview

1) and over the Patagonian Shelf between 40° S and 55° S and between 70° W and 50° W (defined here as Region 2), respectively. The two regions for this study are defined based loosely on dynamic biogeochemical provinces identified using bathymetry, algal biomass, sea surface temperature and salinity (Reygondeau et al., 2013).

Both projects featured en route vertical profiling from near the ocean surface (~ 150 m) to the upper-troposphere, with 74 ORCAS and seven ATom-2 (during the sixth and seventh flights) low-altitude level legs in the MBL. These campaigns shared a number of instruments, including the NCAR Trace Gas Organic Analyzer (TOGA), the NCAR Atmospheric Oxygen (AO2) instrument, a Picarro cavity ringdown spectrometer operated by NOAA, discussed below. More information about individual instruments may be found in Stephens et al., 2018 and at https://www.eol.ucar.edu/field_projects/orcas and <https://espo.nasa.gov/atom/content/ATom>.

2.1.1 Halogenated VOCs

During ORCAS and ATom-2 TOGA provided mixing ratios of over 60 organic compounds, including HVOCs. The instrument, described in Apel et al. (2015), continuously collects and analyzes samples for CHBr_3 , CH_2Br_2 , CHClBr_2 , CHBrCl_2 , and CH_3I among other compounds, with a 35-second sampling period and repeats the cycle every two-minutes using online fast gas chromatography and mass spectrometry. This study also leverages measurements of CH_3Br from whole air samples from the U. Miami / NCAR Advanced Whole Air Sampler (AWAS; Schauffler et al., 1999) onboard the GV during the ORCAS campaign and the UC Irvine Whole Air Sampler (WAS; Blake et al., 2001) onboard the DC-8 during the ATom-2 campaign. HVOCs reported here have an overall $\pm 15\%$ accuracy and $\pm 3\%$ relative precision, and detection limits of 0.03 ppt for CH_3I , 0.2 ppt for CHBr_3 , 0.03 ppt for CH_2Br_2 , 0.03 ppt for CHClBr_2 , 0.05 ppt for CHBrCl_2 , and 0.2 ppt for CH_3Br – 0.2 ppt. In addition, comparisons between onboard collected whole air samples and in-flight TOGA measurements, when sharing over half of their sampling period with TOGA measurements, showed good correlations for CHBr_3 , CH_2Br_2 , CH_3I , and CHClBr_2 , although there were some calibration differences (Fig. S1 and Fig. S2). In addition to the comparison between co-located atmospheric measurements, we also conducted a lab inter-comparison following the campaign between NOAA's programmable flask package (PFP) and TOGA (Table S1; see supplement for details).

2.1.2 $\delta(\text{O}_2/\text{N}_2)$ and CO_2

The AO2 instrument measures variations in atmospheric O_2 , which are reported as relative deviations in the oxygen to nitrogen ratio ($\delta(\text{O}_2/\text{N}_2)$), following a dilution correction for CO_2 (Keeling et al., 1998; Stephens et al., 2018). The instrument's precision is ± 2 per meg units (one in one million relative) for a 5 second measurement (Stephens et al., 2003; Stephens et al., manuscript in preparation, 2019). Anthropogenic, biogenic, and oceanic processes introduce O_2 perturbations that are superimposed on the background concentrations of O_2 in air ($X\text{O}_2$, in dry air = 0.2095). Air-sea O_2 fluxes are driven by both biological production and consumption of O_2 .

Elizabeth Asher 6/16/2019 1:28 PM

Deleted: t

Elizabeth Asher 7/7/2019 10:48 AM

Deleted: 2

Elizabeth Asher 7/5/2019 2:14 PM

Deleted: , at background levels

Elizabeth Asher 7/8/2019 5:29 PM

Deleted: The instrument, described in Apel et al. (2015), continuously collects and analyzes samples

Elizabeth Asher 7/8/2019 5:29 PM

Deleted:

Elizabeth Asher 7/7/2019 11:02 AM

Formatted: Font:Italic

Elizabeth Asher 8/4/2019 2:03 PM

Deleted: 3

Elizabeth Asher 7/7/2019 11:03 AM

Formatted: Subscript

and by heating and cooling of surface waters. O₂ is consumed when fossil fuels are burned and produced and consumed during terrestrial photosynthesis and respiration. Seasonal changes in the ocean heat content lead to small changes in atmospheric N₂. As others have done, we isolated the air-sea O₂ signal by subtracting model estimates of the terrestrial O₂, fossil-fuel O₂, and air-sea N₂ flux influences from the δ(O₂/N₂) measurements (Equation 1; Keeling et al., 1998; Garcia and Keeling, 2001; Stephens et al., 2018). The difference of the δ(O₂/N₂) measurement and these modeled components is multiplied by XO₂ to convert to ppm equivalents as needed (ppm eq; Keeling et al., 1998; Equation 1).

$$O_{2\text{-ppm-equiv}} = [\delta(O_2/N_2) - \delta(O_2/N_2)_{\text{Land}} - \delta(O_2/N_2)_{\text{Fossil Fuel}} - \delta(O_2/N_2)_{N_2}] \times XO_2 \quad (1)$$

We obtained the modeled δ(O₂/N₂) signal terrestrial influences from the land model component of the CESM, the fossil fuel combustion influences from the Carbon Dioxide Information Analysis Center (CDIAC; Boden et al. 2017), and the air-sea N₂ influences from the oceanic component of CESM. These fluxes were all advected through the specified dynamics version of CESM's atmosphere component, as described below in Sect. 2.2 and in Stephens et al. (2018).

CO₂ measurements were provided by NOAA's Picarro G2401-m cavity ring down spectrometer modified to have a ~1.2 sec measurement interval and a lower cell pressure of 80 Torr, which enabled the instrument to function at the full range of GV altitudes. (McKain et al. manuscript in preparation, 2019). Dry-air mole fractions were calculated using empirical corrections to account for dilution and pressure broadening effects as determined in the laboratory before and after the campaign deployments, and in-flight calibrations were used to determine an offset correction for each flight. Corrected CO₂ data have a total average uncertainty of 0.07 ppm (McKain et al. manuscript in preparation, 2019). To merge them with the TOGA data, these faster O₂ and CO₂ measurements were arithmetically averaged over TOGA's 35-s sampling periods (Stephens et al., 2017 and <https://espo.nasa.gov/atom/content/ATom>).

2.2 CAM-Chem model configuration

The CESM version 1, atmospheric component with chemistry (CAM-Chem) is a global three-dimensional chemistry climate model that extends from the Earth's surface to the stratopause. CAM-Chem version 1.2 includes all the physical parameterizations of Neale et al. (2013) and a finite volume dynamical core (Lin, 2004) for tracer advection. The model has a horizontal resolution of 0.9° latitude × 1.25° longitude, with 56 vertical hybrid levels and a time-step of 30 minutes. Meteorology is specified using the NASA Global Modeling and Assimilation Office (GMAO) Goddard Earth Observing System Model, version 5 (GEOS-5; Rienecker et al., 2008) (GEOS-5), following the specified dynamic procedure described by Lamarque et al. (2012). Winds, temperatures, surface pressure, surface stress, and latent and sensible heat fluxes are nudged using a 5-hour relaxation timescale to GEOS-5 1° × 1° meteorology. The sea surface temperature boundary condition is derived from the Merged Hadley-NOAA Optimal Interpolation Sea Surface Temperature and Sea-Ice Concentration product (Hurrell et al., 2008). The model uses chemistry described by Tilmes et al. (2016), biomass burning and biogenic

Elizabeth Asher 6/16/2019 1:28 PM

Deleted: (Keeling et al., 1998; Garcia and Keeling, 2001; Stephens et al., 2018)

Elizabeth Asher 7/7/2019 11:04 AM

Deleted: photosynthesis

Elizabeth Asher 7/7/2019 11:04 AM

Deleted: combustion

Elizabeth Asher 7/7/2019 11:04 AM

Formatted: Subscript

Elizabeth Asher 7/7/2019 11:04 AM

Formatted: Subscript

Elizabeth Asher 7/7/2019 11:05 AM

Deleted: values

Elizabeth Asher 7/8/2019 5:30 PM

Deleted: .

Elizabeth Asher 7/7/2019 11:05 AM

Deleted: land

Elizabeth Asher 7/7/2019 11:09 AM

Deleted: Community Earth System (

Elizabeth Asher 7/7/2019 11:09 AM

Deleted:)

Elizabeth Asher 7/7/2019 11:11 AM

Deleted: 3.1

Elizabeth Asher 8/4/2019 2:04 PM

Deleted: The XO₂ in 2016 is the Tohjima et al. (2005) value from the year 2000 adjusted for the 4 ppm yr⁻¹ or ~20 per meg yr⁻¹ decrease in O₂ between 2000 and 2016.

Elizabeth Asher 7/7/2019 11:11 AM

Deleted: ., in prep., 2019

Elizabeth Asher 7/8/2019 5:30 PM

Deleted: in prep.

emissions from the Fire INventory of NCAR (FINN; Wiedinmyer et al., 2011) and MEGAN (Model of Emissions of Gasses and Aerosols from Nature) 2.1 products (Guenther et al., 2012) and additional tropospheric halogen chemistry described in Fernandez et al. (2014) and Saiz-Lopez et al. (2014). These include ocean emissions of CHBr_3 , CH_2Br_2 , CHBr_2Cl , and CHBrCl_2 , with parameterized emissions based on chlorophyll a ($\text{chl } a$) concentrations and scaled by a factor of 2.5 over coastal regions, as opposed to open ocean regions (Ordoñez et al., 2012). The model used an existing CH_3I flux climatology (Bell et al., 2002), and CH_3Br was constrained to a surface lower boundary condition, also described by Ordoñez et al. (2012). This version of the model was run for the period of the ORCAS field campaign (January and February 2016), following a 24-month spin-up. To facilitate comparisons to ORCAS observations, output included vertical profiles of modeled constituents from the two nearest latitude and two nearest longitude model grid-points (four profiles in total) to the airborne observations at every 30-min model time-step. Following the run, simulated constituent distributions were linearly interpolated to the altitude, latitude and longitude along the flight track, yielding co-located modeled constituents and airborne observations. This version of the model has not yet been run for the ATom-2 period.

2.3 STILT model configuration

The Stochastic Time-Inverted Lagrangian Transport (STILT; Lin et al., 2003) particle dispersion model uses a receptor oriented framework to infer surface sources or sinks of trace gases from atmospheric observations collected downstream, thus simulating the upstream influences that are ultimately measured at the receptor site. The model tracks ensembles of particle trajectories backward in time and the resulting distributions of these particles can be used to define surface influence maps for each observation. STILT was run using 0.5° Global Data Assimilation System (GDAS) reanalysis winds to investigate the transport history of air sampled along the flight track (Stephens et al., 2018). For each TOGA observation, an ensemble of 4,096 particles was released from the sampling location and followed over a backwards simulation period of seven days. Particles in the lower half of the simulated MBL are assigned a surface influence value, which quantitatively links observed mixing ratios to surface sources (Lin et al., 2003). The average surface influence of all 4,096 particles per sampling location yields an hourly and spatially gridded surface influence value ($\text{ppt m}^2 \text{ s pmol}^{-1}$) at a spatial resolution of $0.25^\circ \times 0.25^\circ$ for each sample point.

Uncertainty in the surface influence value is strongly influenced by the accuracy of the underlying meteorological transport, as discussed in Xiang et al. (2010). We evaluated the GDAS reanalysis winds by comparing model winds interpolated in space and averaged between corresponding time points and pressure levels to match aircraft observations. By evaluating observed winds compared with modeled winds along the flight tracks we can estimate uncertainty in the surface influence values. We consider the observation-model differences in both wind speed and direction to approximate errors in surface influence strength and location. For wind speed, a small bias may be present, where we find a median difference between observations and reanalysis of 0.68 m/s, a 5% relative bias. The 1-sigma of the wind speed

difference is 2.3 m/s, corresponding to a 19% 1-sigma uncertainty in wind speed. In its simplest approximation, the surface influence strength error is perfectly correlated with the wind speed error, and thus we take 19% as an approximation of the surface influence strength uncertainty. The uncertainty in surface influence location depends on the error in the wind direction. We find a 1-sigma error of 14 degrees in wind speed, which corresponds to a possible error of 260 km/day.

Finally, we note that photochemical loss during transport is not accounted for in this analysis. Low OH mixing ratios, cold temperatures, and lower photolysis rates due to angled sunlight at high latitudes lead to longer than average HVOC lifetimes. For instance, assuming an average diurnal OH concentration of 0.03 ppt, and average photochemical loss according to the Tropospheric Ultraviolet and Visible (TUV) radiation model and the Mainz Spectral data site (http://satellite.mpic.de/spectral_atlas) for Jan. 29 under clear sky conditions at 60° S, CHBr_3 has a lifetime of 30 days, CH_2Br_2 has a lifetime of 270 days, CH_3I has a lifetime of 7 days, and CHClBr_2 has a lifetime of 63 days. As such, the photochemical lifetimes of these gases are greater than or equal to the time of our back-trajectory analysis. Moreover, OH concentrations in this region have large uncertainties, the inclusion of which would lead to more, not less, uncertainty in surface influence based regression coefficients and estimated fluxes (see Sect. 2.3 and 3.3 for details).

2.3.1 STILT surface influence functions

For this study, we used STILT surface influence distributions with remotely sensed ocean surface and reanalysis data (i.e. surface source fields) in linear and multi-linear regressions to generate empirical STILT influence functions. Surface influence functions can help explain observed mixing ratios of CHBr_3 , CH_2Br_2 , CH_3Br and CH_3I , evaluate the likelihood of particular HVOC sources, and in the case of statistically significant correlations, may be used to derive an estimated flux field (See Sect. 3.3 and 3.4.2 for details).

We tested whether observed mixing ratios (Z) could be explained by a linear relationship in which the predictor variable is a surface influence function, equal to the product of the surface influence (H) and a potential geophysical surface source field(s), such as chl a , as well as an intercept (b), a slope (a), and error term ξ (Equation 2; Fig. S5). This relationship can be generalized as a multiple linear regression with multiple surface influence functions (H_{s_1}, H_{s_2}, \dots) and slope coefficients (a_1, a_2 ; Equation 3), when multiple sources contribute to observed HVOC mixing ratios. The multiple linear regression may also include an interaction term (H_{s_2}) between predictor variables (e.g. H_{s_1} and H_{s_2}) with a slope coefficient (a_3) to improve the fit. Statistical correlations between mixing ratios and surface influence functions may be used to support or reject hypothesized sources. A flux ($\mu\text{mol m}^{-2} \text{s}^{-1}$) may then be estimated for each grid cell based on the product of the slopes (a_1, a_2, \dots) and the potential source fields (s_1, s_2, \dots). Grid cell fluxes are averaged over a geographical region to yield the average regional flux. We used the standard deviation of the regression coefficients and the relative uncertainty in the surface source, added in quadrature, to estimate the uncertainty in the flux (see Sect. 3.4.2 for fractional uncertainties).

469 We note that the uncertainty in STILT transport (see Sect. 2.3 for details) is inherently reflected
470 in the relative uncertainty of the regression coefficients (a_1, a_2, \dots).

471
$$Z = aHs + b + \xi \text{ _____} \quad (2)$$

472
$$Z = a_1Hs_1 + a_2Hs_2 + (a_3Hs_1Hs_2) \dots + b + \xi \text{ _____} \quad (3)$$

473

474 **2.3.2 Surface Source Fields**

475 Geophysical surface source fields of remotely sensed and reanalysis data included a combination
476 of sea ice concentration, chl a , absorption due to ocean detrital material, and downward
477 shortwave radiation at the ocean surface.

478 We used daily sea ice concentration data (<https://nsidc.org/data/nsidc-0081>) at a 25 km x 25 km
479 spatial resolution between 39.23° S and 90° S, 180° W – 180° E from the NASA National Snow
480 and Ice Data Center Distributed Active Archive Center (NSIDC; Maslanik et al., 1999). This
481 data reports the fraction of sea-ice cover, land-ice cover, and open water. Unfortunately, these
482 data do not provide any information on sea ice thickness, or the presence of brine channels or
483 melt ponds, which may modulate emissions from sea-ice covered regions. Sea ice concentration
484 data were calculated using measurements of near-real-time passive microwave brightness
485 temperature from the Special Sensor Microwave Image/Sounder (SSMIS) on the Defense
486 Meteorological Satellite Program (DMSP) satellites. NSIDC sea ice concentration data were
487 arithmetically averaged to yield 0.25° x 0.25° binned sea ice fraction for use with gridded surface
488 influences.

489 Due to persistent cloud cover over the Southern Ocean, which often precludes the retrieval of
490 remotely sensed ocean color data, we used 8-day mean composite Aqua MODIS L3 distributions
491 of chl a from the Ocean Color Index (OCI) algorithm and absorption due to gelbstoff and detrital
492 material at 443 nm from the Generalized Inherent Optical Properties (GIOP) model (NASA
493 Goddard Space Flight Center, 2014). Absorption due to gelbstoff and detrital material at 443 nm
494 is used as a proxy for colored dissolved organic matter (CDOM;
495 <https://oceancolor.gsfc.nasa.gov/atbd/giop/>). CDOM is hypothesized to be an important source of
496 carbon for the photochemical production of CH_3I (Moore et al., 1994). The GIOP model also
497 publishes an uncertainty in the absorption due to gelbstoff and detrital material at 443 nm. Raw
498 4 km x 4 km data were geometrically averaged, based on lognormal probability density
499 functions, to a spatial resolution of 0.25° x 0.25° for use with gridded surface influences. We
500 used the ratio of the 0.25° x 0.25° gridded uncertainty in the detrital material absorption to the
501 absorption as the relative uncertainty for flux calculations (see Sect. 3.4.2).

502 The National Center for Environmental Prediction (NCEP) provides Final Global Data
503 Assimilation System (GDAS/FNL) global data of downward shortwave radiation at the surface
504 at 0.25 degree and 6-hour resolution (NCEP, 2015). We chose downward shortwave radiation
505 for use with gridded surface influences because the photo-production of CH_3I has been observed
506 at all visible wavelengths (Moore et al., 1994). This reanalysis data is available at a higher

Elizabeth Asher 7/5/2019 2:55 PM

Formatted: Font:

temporal resolution and better spatial coverage than satellite retrievals of photosynthetically active radiation (PAR) or temperature.

3 Results and discussion

3.1 Observed HVOC patterns and relationships

Zonal cross-sections of HVOC data collected on ORCAS and ATom-2 illustrate unprecedented spatial sampling across our study area between the surface and 12 km (Fig. 2). Above average mixing ratios of CH₃I, CHBr₃, and CHClBr₂ typically remain confined to the lower ~2-4 km of the atmosphere (Fig. 2a, b, d). These compounds have lifetimes of approximately two months or less. Conversely, weak sources and longer lifetimes (≥ 3 months) may have contributed to similar concentrations of CH₂Br₂ and CHBrCl₂ throughout the troposphere and above average mixing ratios as high as 8 km (Fig. 2c, e). Unfortunately, the availability of data above the detection limit and absence of BL enhancements for CHBrCl₂ preclude the identification of strong regional sources at this time. Meridional distributions also indicate lower latitude sources of CH₃I and CH₃Br ($< 50^\circ$ S), potentially resulting from terrestrial and anthropogenic contributions, and higher latitude sources ($> 60^\circ$ S) of CHBr₃, CH₂Br₂, and CHClBr₂ (Fig. 2a-d,f).

3.1.1 Observed HVOC interrelationships

Across our study area in both 2016 and 2017, we found that CHBr₃ and CH₂Br₂ exhibit a consistent enhancement ratio with each other in the bottom 2 km of the atmosphere both in Region 1 and Region 2, which suggests that these bromocarbon fluxes are closely coupled. Previous studies have documented co-located source regions of CHBr₃ and CH₂Br₂ in the Southern Ocean (e.g. Hughes et al., 2009; Carpenter et al., 2000; Nightingale et al., 1995; Laturnus et al., 1996), and laboratory studies have demonstrated that phytoplankton and their associated bacteria cultures, including a cold water diatom isolated from coastal waters along the Antarctic Peninsula and common to the Southern Ocean, produce both CHBr₃ and CH₂Br₂ (Hughes et al., 2013; Tokarczyk and Moore 1994, Sturges et al., 1993). The non-linearity observed in ratios of these two gases at low CHBr₃ may reflect the different rates of their production or loss in seawater, or possibly, the influence of air masses from distant, more productive low-latitude source regions. Several studies have documented bacterially mediated loss of CH₂Br₂, but not CHBr₃, and report distinct ratios of CH₂Br₂ to CHBr₃ in seawater during the growth and senescent phases of a phytoplankton bloom (e.g. Carpenter et al., 2009, Hughes et al., 2013). Although this analysis is restricted to the bottom 2 km of the atmosphere, zonal transport of air masses with lower ratios of CH₂Br₂ to CHBr₃ ratios, as have been observed in the MBL over productive, low-latitude regions, may also have influenced our observations (Yokouchi et al. 2005). Mixing ratios of CHBr₃ and CHClBr₂ were also correlated (Fig. 3d) in Region 2, and, a similar, weaker relationship was observed in Region 1 (Fig. 3b). CHClBr₂ is a

Elizabeth Asher 7/7/2019 11:15 AM

Deleted: ,

Elizabeth Asher 7/7/2019 11:16 AM

Deleted: and d

Elizabeth Asher 7/7/2019 11:16 AM

Deleted: (\geq

Elizabeth Asher 7/7/2019 11:16 AM

Deleted: -

Elizabeth Asher 7/7/2019 11:16 AM

Deleted: \leq -

Elizabeth Asher 7/7/2019 2:46 PM

Formatted: Font:Bold

Elizabeth Asher 7/8/2019 5:34 PM

Deleted: (Fig. 3a, c)

less well-studied compound than CH₂Br₂. Yet these consistent relationships suggest that CHBr₃ and CHClBr₂ may either share some of the same sources or have sources that co-vary.

553

3.1.2 Observed HVOC relationships to $\delta(\text{O}_2/\text{N}_2)$ and CO₂

We sought to test if the biologically mediated production of bromocarbons and oxygen result in similar atmospheric distributions. Conversely, we expected HVOC atmospheric distributions and CO₂ distributions to anticorrelate because CO₂ fixation in surface waters is proportional to the production of oxygen.

For these comparisons, both O₂ and CO₂ mixing ratios from the upper troposphere (5-7 km) were subtracted from the data to detrend for seasonal and inter-annual variability (Fig. 4; Fig. S3). To isolate the contribution of ocean O₂ fluxes, the ORCAS $\delta(\text{O}_2/\text{N}_2)$ values reported here represent the $\Delta\delta(\text{O}_2/\text{N}_2)$ to observed values between 5-7 km adjusted for CESM O₂ land and fossil fuel contributions and the influence of air-sea N₂ fluxes. In Fig. 4 we present type II major axis regression fits to data (fits were calculated using data scaled to their full range) between the ocean surface and the lowest 7 km for bromocarbons with photochemical lifetimes of ≥ 1 month and from the lowest 2 km for CH₃I with a photochemical lifetime of ~ 1 week. We used a type II major axis regression model to balance the influences of uncorrelated processes and measurement uncertainty in HVOCs (on the y-axis) and uncorrelated processes and measurement uncertainty in O₂ and CO₂ (on the x-axis) on the regression slope (Ayers et al., 2001; Glover et al., 2011). As noted by previous studies, simple least squares linear regressions fail to account for uncertainties in predictor variables (e.g. Cantrell et al., 2008).

The robust correlations of CHBr₃ and CH₂Br₂ with $\delta(\text{O}_2/\text{N}_2)$, in both 2016 and 2017 and in Region 1 and Region 2, provides support for a regional biogenic source of these two HVOCs (Fig. 4a, b and Fig. 4d, e). The air-sea exchange of O₂ during summer in the Southern Ocean is driven by net community production (the excess of photosynthesis over respiration) in the surface mixed layer, surface warming, and to a lesser extent ocean advection and mixing (e.g. Stephens et al., 1998; Tortell and Long 2009; Tortell et al., 2014). Note that we adjust for influences on the $\delta(\text{O}_2/\text{N}_2)$ from thermal N₂ fluxes (see Equation 1, Sect. 2.1.2 for details). Biological O₂ supersaturation in the surface mixed layer develops quickly in the first several days of a phytoplankton bloom and diminishes as community respiration increases and air-sea gas exchange equilibrates the surface layer with the atmosphere on a timescale of ~ 1 week. CHBr₃ and CH₂Br₂ are emitted from phytoplankton during the exponential growth phase (Hughes et al., 2013), which often coincides with high net community production and the accumulation of O₂ in surface waters. The bulk air-sea equilibration time for an excess of CHBr₃ and other HVOCs is less than two weeks, although the photochemical loss of HVOCs will alter their ratio over time (see Supplement for details on calculations of bulk sea air equilibration times).

Our observations suggest a biological source for CHBr₃ and CH₂Br₂ in both Region 1 and Region 2 (Fig. 4). Interestingly, the slope of the regression between CHBr₃ and O₂ appears distinct in Region 1 and Region 2, but between CH₂Br₂ is the same. Molar enrichment ratios are $0.20 \pm$

Elizabeth Asher 7/5/2019 2:24 PM

Deleted: 2.5

Elizabeth Asher 7/7/2019 11:17 AM

Deleted:

Elizabeth Asher 7/8/2019 5:43 PM

Deleted: (bivariate)

Elizabeth Asher 7/7/2019 11:28 AM

Deleted: the

Elizabeth Asher 7/7/2019 11:28 AM

Deleted: oxygen

Elizabeth Asher 7/7/2019 11:28 AM

Formatted: Subscript

Elizabeth Asher 7/7/2019 11:29 AM

Deleted: 3

Elizabeth Asher 7/7/2019 11:29 AM

Deleted: (

Elizabeth Asher 7/7/2019 11:29 AM

Deleted:) is

0.01, and 0.07 ± 0.004 pmol : mol for CHBr_3 and CH_2Br_2 to O_2 in Region 1, and 0.32 ± 0.02 , and 0.07 ± 0.004 pmol : mol in Region 2. We observe a weaker relationship between CH_3I and CHClBr_2 and O_2 in Region 1 (Fig. 4c, d), consistent with the existence of other, non-biological sources of CH_3I in this region. Figure 4f illustrates a strong relationship between CH_3I and O_2 , as well as CHClBr_2 and O_2 , in Region 2, however, which implies that the dominant sources of CH_3I and CHClBr_2 emissions over the Patagonian Shelf are biological. The corresponding molar enrichment ratios of CH_3I to O_2 and CHClBr_2 to O_2 in Region 2 are 0.38 ± 0.03 pmol : mol and 0.19 ± 0.04 pmol : mol, respectively.

In contrast to O_2 , air-sea fluxes of CO_2 over the Southern Ocean during summer reflect the balance of opposing thermal and biological drivers (e.g. Stephens et al., 1998; 2018). Ocean buffering chemistry results in CO_2 equilibration across the air-sea interface on a timescale of several months. ORCAS observations showed a depletion of CO_2 in the MBL, indicating that uptake driven by net photosynthesis dominated over thermally driven outgassing during the several months preceding the campaign (Stephens et al., 2018). CHBr_3 and CH_2Br_2 in the lowest 7 km were negatively correlated with CO_2 in both years in Region 1 and Region 2 (Fig. S3a, b, d, e). Interestingly, CH_3I was not correlated with CO_2 in Region 1, likely due to the long air-sea equilibration timescale of CO_2 compared with a 9-day air-sea equilibration time and a ~ 7 -day photochemical lifetime for CH_3I . For longer lived species, correlations for HVOCs to CO_2 have similar r^2 -values as those for HVOCs to $\delta(\text{O}_2/\text{N}_2)$, but model and climatological estimates of Southern Ocean CO_2 fluxes are much less certain than for O_2 (Anav et al., 2015; Nevison et al., 2016). As a result, we use modeled O_2 fluxes as the basis for our HVOC flux estimates (see Sect. 3.4.1 for details).

3.2 Model-observation comparisons

The ORCAS dataset provides an exceptional opportunity to evaluate the CAM-Chem HVOC emission scheme (Ordoñez et al., 2012) at high latitudes in the Southern Hemisphere. We compared modeled HVOC constituents to corresponding observations along the ORCAS flight track (Fig. 5; Fig. 6). In these figures, we used type II major axis regression models to balance the measurement uncertainty (on the y-axis) and the inherent, yet difficult to quantify representativeness and errors in a global atmospheric chemistry model (on the x-axis). We note that this comparison may favor constituents with longer photochemical lifetimes, when transport and mixing dominate over source heterogeneity.

In Region 1 and Region 2, both the model and observations indicate that elevated mixing ratios of CH_3I remain confined to the MBL (Fig. 5a and Fig. 6a), presumably due to its relatively short photochemical lifetime. Modeled and observed CH_3I are poorly correlated in Region 1 ($r^2 = 0.20$; Fig. 5b) and better correlated in Region 2 ($r^2 = 0.70$; Fig. 6b). In both regions, the model underpredicts CH_3I in the upper troposphere and lower stratosphere (UTLS), likely stemming from the poleward transport of lower latitude air masses, where CAM-Chem also exhibits a negative bias. Mixing ratio comparisons with CAM-Chem over the tropics (see Figure 10 in Ordoñez et al., 2012) depict similar or larger discrepancies, and have been attributed to stronger

Elizabeth Asher 7/7/2019 11:31 AM
Deleted: s

Elizabeth Asher 7/8/2019 5:44 PM
Deleted:

641 | than anticipated convective cells in the tropics. We found strong correlations and agreement to
 642 | within a factor of ~2 between modeled and observed CHBr_3 and CH_2Br_2 (Fig. 5c-f and Fig. 6c-f).
 643 | Relatively long lifetimes (≥ 1 month) in Region 1 likely enable vertical and zonal transport of
 644 | CHBr_3 and CH_2Br_2 to the mid and upper troposphere (Fig. 5c and e). The model was biased low
 645 | with respect to measurements of CH_3Br by ~25% in Region 1 and Region 2 (Fig. 5g-h and Fig.
 646 | 6g-h), potentially as a result of an incorrect surface lower boundary condition. The model
 647 | underpredicted the mean vertical gradient in CHClBr_2 , although it did a reasonable job of
 648 | representing the mean vertical gradient in CHBrCl_2 , in both Region 1 and Region 2. In both
 649 | cases, however, the model failed to capture the spatial variability in both CHClBr_2 and CHBrCl_2
 650 | observations (Fig. 5i-l and Fig. 6i-l). Region 2 contains stronger sources of HVOCs than Region
 651 | 1, which has been documented in numerous ship-based campaigns and archived in the
 652 | Halocarbons in the Ocean and Atmosphere database (HalOcAt; <https://halocat.geomar.de/>).
 653 | Region 2 also has much higher chl *a* (Fig. S4), supporting biogenic sources for these gases.

654

655 | **3.3 Relationships between STILT surface influence functions and observations**

656 | We used the STILT model to explore the relationships between observed mixing ratios and the
 657 | upstream surface influence functions (Equations 2-3) of sea ice, chl *a*, absorption due to detritus,
 658 | and downward shortwave radiation at the surface, which relate to various regional hypothesized
 659 | sources of HVOCs such as marine phytoplankton, phytoplankton in sea ice brines, and
 660 | decomposing organic matter in surface seawater (e.g. Moore and Zafiriou 1994; Moore et al.,
 661 | 1996; Tokarczyk and Moore 1994; Sturges et al., 1992).

662

663 | We found no positive relationships between upstream sea-ice influence and any measured
 664 | HVOC Region 1 (Fig. 7). We interpret this result to mean that increased summertime sea ice acts
 665 | either to reduce the production of HVOCs by blocking sunlight or as a physical barrier to oceanic
 666 | emissions of HVOCs from under-ice algae. Both of these mechanisms are also consistent with a
 667 | link between enhanced CHBr_3 and CH_2Br_2 emissions due to sea-ice retreat and surface sea-ice
 668 | melt water (Carpenter et al., 2007).

669 | In other studies, it has also been proposed that sea ice could be an important source for CHBr_3
 670 | and other HVOCs, since high mixing ratios of CHBr_3 have been observed at the sea-ice and ice-
 671 | snow interface in the austral winter (Abrahamsson et al., 2018) and in under-ice algae in the
 672 | austral spring (Sturges et al., 1993). At present, CAM-Chem v1.2 with very short-lived halogen
 673 | chemistry does not include a regional flux of HVOCs over sea-ice covered waters in summer,
 674 | and our results do not indicate a need to include one. Our data, which were collected in January
 675 | and February, however, cannot assess the importance of sea ice as a source of HVOCs in other
 676 | seasons, such as winter or spring (Abrahamsson et al., 2018; Sturges et al., 1993). More field
 677 | campaigns are needed to further study the seasonality and regional strength of sea ice related
 678 | HVOC emissions.

Elizabeth Asher 7/7/2019 11:37 AM

Deleted:

Elizabeth Asher 7/7/2019 11:44 AM

Deleted: . High concentrations of CHBr_3 have been linked to sea ice retreat

682 We observed a statistically significant positive correlation between the surface influence function
 683 of 8-day satellite composites of chl *a* concentration, which is widely used as a proxy for near-
 684 surface phytoplankton biomass, and mixing ratios of CHBr₃ and CH₂Br₂ in Region 1 (Fig. 8a, b).
 685 This finding corroborates previous findings from ship-borne field campaigns and laboratory
 686 studies that have suggested a biogenic source for these two bromocarbons (e.g., Moore et al.,
 687 1996; Hughes et al., 2013), and further substantiates the current CAM-Chem parameterization of
 688 regional bromocarbon emissions using satellite retrievals of chl *a* in polar regions. CH₃Br
 689 mixing ratios were not significantly correlated with chl *a* surface influence functions (Fig. 8c).
 690 Although potentially suggesting that marine phytoplankton and microalgae were not a strong
 691 regional source of CH₃Br during ORCAS, it is also possible that the relatively long lifetime of
 692 CH₃Br precludes a definitive analysis of its origin based on chl *a* using 7-day back-trajectories.
 693 Neither CHClBr₂ nor CHBrCl₂ were significantly correlated with chl *a* composite surface
 694 influence functions (data not shown); however, more observations of these short-lived species in
 695 the remote MBL are needed to substantiate this result.

696 Similar to Lai et al. (2011), we observed a significant correlation between mixing ratios of CH₃I
 697 and total weekly upstream influence functions of 8-day chl *a* composites (Fig. 8d). Weaker
 698 correlations were observed with upstream influence functions on shorter timescales than seven
 699 days. We found that CH₃I, particularly in Region 1, was better explained by a multi-linear
 700 regression with two predictors: 1) the influence function of downward shortwave radiation at the
 701 surface (Fig. 9a) and 2) the absorption of light due to detrital material (Fig. 9b), yielding
 702 improved agreement between predicted and observed CH₃I (Fig. 9c). Several previous studies
 703 have correlated mixing ratios of CH₃I to satellite retrievals of PAR and surface ocean
 704 temperature, revealing a link to solar radiation (e.g. Happell et al., 1996; Yokouchi et al., 2001).

705 Although certain species of phytoplankton are capable of producing CH₃I (e.g. Manley and de la
 706 Cuesta 1997; Hughes et al., 2011), several studies also indicate a non-biological source for CH₃I
 707 in the surface ocean. This non-biological source, though not fully understood, requires light, a
 708 humic like substance at the surface ocean supplying a carbon source and methyl group, and
 709 reactive iodine (Moore and Zarifou 1994; Richter and Wallace 2004). Thus far, two chemical
 710 mechanisms have been proposed for the non-biological production of methyl iodide, one – a
 711 radical recombination of a methyl group and iodine involving UV photolysis (e.g. Moore and
 712 Zarifou 1994), and two, a substitution reaction involving the reduction of an oxidant, such as iron
 713 III (e.g. Williams et al. 2007).

714

715 **3.4 Flux estimation**

716 **3.4.1 O₂-based emission estimates**

717 We present a novel approach that facilitates a basin-wide HVOC flux estimate using the robust
 718 relationship between airborne observations of O₂ and HVOCs combined with modeled O₂ fluxes.
 719 Unlike the existing CAM-Chem HVOC biogenic flux parameterization, this method does not
 720 rely on weekly retrievals of chl *a* at high latitudes, which are often patchy. In addition, our study

Elizabeth Asher 7/8/2019 3:54 PM

Deleted: footprints

Elizabeth Asher 7/7/2019 11:44 AM

Deleted: the

Elizabeth Asher 7/7/2019 11:44 AM

Deleted: and Fig. 8

Elizabeth Asher 7/8/2019 3:54 PM

Deleted: footprints

Elizabeth Asher 7/7/2019 11:44 AM

Deleted:

Elizabeth Asher 7/8/2019 3:55 PM

Deleted: footprints

Elizabeth Asher 8/4/2019 4:08 PM

Deleted:

Elizabeth Asher 8/4/2019 4:08 PM

Deleted: Several previous studies have correlated mixing ratios of CH₃I to satellite retrievals of PAR and temperature (e.g. Happell et al., 1996; Yokouchi et al., 2001). We note that chl *a*, which is a proxy for living algal biomass, was correlated with CDOM in Region 1 and Region 2, ($r^2 = 0.24$; data not shown).

736 indicates that CHBr_3 , CH_2Br_2 , and CHClBr_2 and CH_3I are better correlated with marine derived
737 O_2 than the upstream influence of chl a .

738 For CHBr_3 , CH_2Br_2 , and CHClBr_2 we construct ocean emission inventories for January and
739 February using a scaled version of gridded modeled air-sea O_2 fluxes and the slopes (i.e. molar
740 ratios) of linear correlations between $\delta(\text{O}_2/\text{N}_2)$ and HVOC mixing ratios (Fig. 10). O_2 fluxes
741 were obtained from simulations using a configuration of the CESM model nudged to reanalysis
742 temperatures and winds as described in Stephens et al. (2018). An earlier free running version of
743 CESM was one of the best evaluated for reproducing the seasonal cycle of $\delta(\text{O}_2/\text{N}_2)$ over the
744 Southern Ocean (Nevinson et al., 2015; 2016). To date, the north-south gradient in atmospheric
745 O_2 has not been well reproduced by any models (Resplandy et al., 2016). Vertical gradients in O_2
746 on ORCAS indicate that CESM overestimated gradients by 47% on average; accordingly, O_2
747 fluxes were adjusted downward by 47% to better match the observations. This is obviously a
748 very simple adjustment to the modeled fluxes, and the actual air-sea O_2 flux biases in CESM
749 likely have a great deal of spatial and temporal heterogeneity. We calculated an uncertainty for
750 the CESM flux using a second, independent estimate of O_2 fluxes based on dissolved O_2
751 measurements in surface seawater. The Garcia and Keeling (2001) climatology has much
752 smoother temporal and spatial patterns than CESM flux estimates but also results in
753 overestimated atmospheric O_2 spatial gradients. We calculate the relative uncertainty in O_2 flux
754 as the ratio of the mean absolute difference between gridded Garcia and Keeling values (2001;
755 also adjusted down by 51 % everywhere to better match ORCAS observations) to the CESM
756 model flux estimates in Regions 1 and 2 (adjusted down by 47% everywhere). These
757 disagreements were 7.3 % and 3.4 % for Regions 1 and 2, respectively. Based on the ratios of
758 HVOC to O_2 mixing ratios in bivariate least squares regressions and these adjusted O_2 fluxes, we
759 estimate mean emissions of CHBr_3 and CH_2Br_2 in Region 1 and Region 2. Relative uncertainty
760 in the slopes (i.e., the standard deviation of the slopes) from these regressions and the mean
761 relative uncertainties in regional O_2 fluxes were added in quadrature to yield uncertainties in
762 calculated HVOC emission rates.

763
764 Figure 10 shows the mean emissions for Jan. and Feb. of CHBr_3 , CH_2Br_2 , and CHClBr_2 in
765 Region 1 and Region 2. Mean regional emissions of CHBr_3 and CH_2Br_2 and CHClBr_2 are 91 ± 8 ,
766 31 ± 17 , and 11 ± 4 $\text{pmol m}^{-2} \text{hr}^{-1}$ in Region 1 and 329 ± 23 , 69 ± 5 , and 24 ± 5 $\text{pmol m}^{-2} \text{hr}^{-1}$ in
767 Region 2 (Table 1). The mean flux of CH_3I in Region 2 is 392 ± 32 (Table 1). Table 1 also lists
768 the mean Jan. and Feb. CAM-Chem emissions from Region 1 and Region 2, as well as emissions
769 from several other observational and modeling Antarctic polar studies. Our estimates fall within
770 the range of these other studies, which span every month of the year and whose estimated fluxes
771 range from negative (i.e. from the atmosphere into the ocean) to $3500 \text{ pmol m}^{-2} \text{hr}^{-1}$ CHBr_3 in a
772 coastal bay during its peak in primary production. CAM-Chem emissions for all species are
773 significantly lower than our observationally derived values in Region 1, with the exception of
774 CH_3I . Conversely, CAM-Chem emissions are significantly higher than our estimated emissions
775 in Region 2, with the exception of CHClBr_2 in Region 1, which remains underpredicted by the

Elizabeth Asher 7/8/2019 5:45 PM

Deleted: to facilitate comparisons across regions and atmospheric models

Elizabeth Asher 7/7/2019 11:47 AM

Deleted: O_2/N_2

Elizabeth Asher 7/7/2019 11:49 AM

Deleted: Region

Elizabeth Asher 7/7/2019 11:49 AM

Deleted: (7.3% in Region 1 and 3.4 % in Region 2)

Elizabeth Asher 7/7/2019 11:50 AM

Deleted: Antarctic polar

Elizabeth Asher 7/7/2019 11:50 AM

Deleted: biological

Elizabeth Asher 7/8/2019 5:46 PM

Deleted:

785 model (Table 1). We note that in Region 2, CAM-Chem fluxes of CHBr_3 and CH_2Br_2 , although
786 still significantly different, are more similar to our estimated fluxes.

787

788 3.4.2 STILT-based emission estimates

789 Similar to our O_2 -based emission estimates, we used the relationship between surface influence
790 functions and CH_3I mixing ratios (Fig. 9) to predict a flux field in Region 1 (Fig. 11). We used a
791 multiple linear regression (± 1 standard deviations; Equation 2), where H_{s1} and H_{s2} are the
792 downward shortwave radiation and detrital absorption surface influence functions, respectively,
793 with an intercept $b = 0.19 \pm 0.01$, and influence coefficients $a_1 = 3.7\text{E-}5 \pm 1.3\text{E-}5$, $a_2 = 3.5 \pm 0.74$,
794 and an interaction term with the coefficient $a_3 = -5.2\text{E-}4 \pm 1.5\text{E-}4$ (Fig. 9c). These regression
795 coefficients and interaction term were used to estimate an average non-biological flux of CH_3I
796 (Fig. 11; Table 1). This method could be used in place of the current Bell et al. (2002)
797 climatology to update near weekly (~8 day) emissions of CH_3I in future versions of CAM-Chem.
798 Our estimated mean CH_3I flux in Region 1 ($35 \pm 29 \text{ pmol m}^{-2} \text{ hr}^{-1}$) is significantly lower than the
799 current CAM-Chem estimated emissions (Table 1). As noted in Sect. 3.2, our observations of
800 CH_3I are also much lower than the modeled mixing ratios. As discussed above, the strong
801 correlations between CH_3I and O_2 in Region 2 also suggest a dominant biological source for this
802 compound in this region. As a result, we have not used this relationship to parameterize a flux
803 for CH_3I in Region 2 (see Sect. 3.1.2 and 3.4.1 for details). We note that although it would be
804 possible to provide STILT-based emission estimates for other HVOCs (e.g. CHBr_3 and CH_2Br_2),
805 the correlations these compounds were less strong with surface influence functions than those
806 with O_2/N_2 .

807

808 4 Conclusions

809 Our work combined TOGA and AWAS HVOC airborne observations from the ORCAS and
810 ATom-2 campaigns, with coincident measurements of O_2 and CO_2 , geophysical datasets and
811 numerical models, including the global atmospheric chemistry model CAM-Chem, and the
812 Lagrangian transport model, STILT. We evaluated model predictions, calculated molar
813 enrichment ratios, inferred regional sources, and provided novel means of parameterizing ocean
814 fluxes. We found that the Southern Ocean MBL is enriched in HVOCs, but that these MBL
815 enhancements are less pronounced at higher latitudes, i.e., poleward of 60° S (Region 1) than
816 over the productive Patagonian shelf (Region 2). Overall, our results indicated that the Southern
817 Ocean is a moderate regional sources of CHBr_3 , CH_2Br_2 , and CH_3I , and a weak source of
818 CHClBr_2 and CHBrCl_2 in January and February. Good model-measurement correlations were
819 obtained between our observations and simulations from the Community Earth System Model
820 (CESM) atmospheric component with chemistry (CAM-Chem) for CHBr_3 , CH_2Br_2 , CH_3I , and
821 CHClBr_2 but all showed significant differences in model:measurement ratios. The
822 model:measurement comparison for CH_3Br was satisfactory and for CHBrCl_2 the low levels
823 present precluded us from making a complete assessment.

824 CHBr_3 and CH_2Br_2 exhibited strong and robust correlations with each other and with O_2 and
825 weaker but statistically significant correlations with the influence of chl a , which is a proxy for

Elizabeth Asher 7/7/2019 11:52 AM

Formatted: Subscript

Elizabeth Asher 7/7/2019 11:53 AM

Deleted: The shortwave radiation and detrital material influence function

Elizabeth Asher 7/7/2019 11:53 AM

Deleted: an

Elizabeth Asher 7/7/2019 11:53 AM

Deleted: from a multi-linear regression (Fig. 9)

Elizabeth Asher 7/7/2019 11:53 AM

Deleted: regional

Elizabeth Asher 7/7/2019 11:54 AM

Deleted: .

Elizabeth Asher 7/7/2019 11:55 AM

Formatted: Subscript

Elizabeth Asher 7/7/2019 11:55 AM

Formatted: Subscript

Elizabeth Asher 7/7/2019 11:55 AM

Formatted: Subscript

Elizabeth Asher 7/7/2019 11:55 AM

Deleted: 6

Elizabeth Asher 7/7/2019 11:56 AM

Deleted: climate model

Elizabeth Asher 7/8/2019 5:49 PM

Deleted: and

Elizabeth Asher 7/8/2019 5:49 PM

Deleted:

Elizabeth Asher 7/8/2019 5:49 PM

Deleted: in Region 1 (at higher latitudes) than in Region 2 over the productive Patagonian shelf

Elizabeth Asher 7/8/2019 5:50 PM

Deleted: poleward of 60° S (Region 1) and Patagonian Shelf (Region 2) are

Elizabeth Asher 7/8/2019 5:50 PM

Deleted: s

Elizabeth Asher 7/8/2019 5:53 PM

Deleted:

844 phytoplankton biomass. CHClBr_2 and CHBr_3 were well correlated with one another, particularly
845 in Region 2. Together, these correlations suggested a biological source for these gases over the
846 Southern Ocean. We found that CH_3I mixing ratios in Region 1 were best correlated with a non-
847 biological surface influence function, although biogenic CH_3I emissions appear important in
848 Region 2.

849
850 Our flux estimates based on the relationship of HVOC mixing ratios to O_2 and remotely sensed
851 parameters (for CH_3I) were compared with those derived from global models and ship-based
852 studies (Table 1). Our emission estimates of CHBr_3 , CH_2Br_2 , and CHClBr_2 are significantly
853 higher than CAM-Chem's globally prescribed emissions in Region 1, where HVOC mixing
854 ratios are under predicted (Table 1; Fig. 5). Similarly, our estimate of CHClBr_2 emissions is also
855 significantly higher than CAM-Chem's in Region 2, where CHClBr_2 mixing ratios remained
856 underpredicted. Yet, to the best of our knowledge, CAM-Chem's global parameterization of
857 HVOC fluxes has not been compared with data at high latitudes. Indeed, our emission estimates
858 of CHBr_3 , CH_2Br_2 , CH_3I fall within a range of CAM-Chem's estimates (on the low end) and
859 most prior estimates based on either other models or localized studies using seawater-side
860 measurements from the Antarctic polar region in summer (on the high end). In the case of CH_3I ,
861 our estimated emissions suggest that the prescribed emissions in CAM-Chem may be too high in
862 Region 1 and Region 2. Our parameterizations of the CH_3I flux could be used to explore inter-
863 annual variability in emissions, which is not captured by the Bell et al. (2002) CH_3I climatology
864 currently employed in CAM-Chem.

865 To extend these relationships to year-round and global parameterizations for use in global
866 climate models, they must be studied using airborne observations in other seasons and regions.
867 These approaches may help parameterize emissions of new species that can be correlated with
868 surface influence functions or the biological production of oxygen or may improve existing
869 emissions, where persistent biases exist. Finally, future airborne observations of HVOCs have
870 the potential to further improve our understanding of air-sea flux rates and their drivers for these
871 chemically and climatically important gases over the Southern Ocean.

872 **Data Availability.** The ORCAS and ATom-2 datasets are publicly available at
873 <https://doi.org/10.5065/D6SB445X>; (www.eol.ucar.edu/field_projects/orcas) and
874 <https://doi.org/10.3334/ORNLDAAAC/1581>.

875 **Author Contributions.** EA is responsible for the bulk of the conceptualization, formal analysis,
876 writing, review, and editing with contributions from all authors. BBS and ECA were
877 instrumental in the investigation and supervision related to this manuscript. RSH contributed to
878 the conceptualization, as well as the investigation and HVOC data curation for this project. BBS,
879 EJM, and RFK were responsible for the data curation of $\delta(\text{O}_2/\text{N}_2)$ data and contributed to formal
880 analysis involving these data. MSHM along with EAK were responsible for STILT data curation
881 and formal analysis, and the conceptualization and formal analysis of SITLT-based geostatistical
882 influence functions and flux estimates were also informed by these two. DK, along with ST, JFL
883 and ASL were responsible for constructing CAM HVOC emissions and conducting CAM runs.
884 MCL was responsible for CESM simulations yielding O_2 fluxes and comparing this product
885 alongside the Garcia and Keeling O_2 climatology in CAM. KMC and CM were responsible for
886 the data curation of CO_2 observations. AJH contributed to the investigation for HVOC data.

Elizabeth Asher 7/8/2019 5:53 PM

Deleted: CAM-Chem provided a good foundation for HVOC, particularly for CHBr_3 and CH_2Br_2 in Region 1 and Region 2. Conversely, CHClBr_2 and CHBrCl_2 were underestimated by a factor of two or three in the model, while CH_3I were overestimated by a factor of more than three, and airborne observations indicated that the CAM-Chem CH_3Br surface boundary condition may be too low by ~25%. ... [1]

Elizabeth Asher 7/8/2019 5:53 PM

Formatted: Subscript

Elizabeth Asher 7/8/2019 5:53 PM

Deleted: other airborne observations

Elizabeth Asher 7/8/2019 5:54 PM

Deleted: relatively well

Elizabeth Asher 7/7/2019 12:02 PM

Deleted: emission estimates of CHBr_3 , CH_2Br_2 , CH_3I , lower than most prior estimates from the Antarctic polar region in summer

Elizabeth Asher 7/7/2019 12:10 PM

Deleted: Nevertheless,

Elizabeth Asher 7/7/2019 12:10 PM

Deleted: t

Elizabeth Asher 7/7/2019 12:29 PM

Deleted:

Elizabeth Asher 7/7/2019 12:30 PM

Deleted:

Elizabeth Asher 7/7/2019 12:30 PM

Deleted: (

Elizabeth Asher 7/7/2019 12:31 PM

Deleted:)

Elizabeth Asher 7/7/2019 12:31 PM

Deleted: (

Elizabeth Asher 7/7/2019 12:31 PM

Deleted:)

Elizabeth Asher 7/7/2019 12:33 PM

Deleted: O_2/N_2

912

913 *Acknowledgements.* We would like to thank the ORCAS and ATom-2 science teams and the
914 NCAR Research Aviation Facility and NASA DC-8 pilots, technicians and mechanics for their
915 support during the field campaigns. In addition, we appreciate the NCAR EOL staff who have
916 facilitated computing and data archival. In particular, we thank Tim Newberger for his help in
917 supporting the NOAA Picarro CO₂ observations and Andrew Watt for his help in supporting the
918 AO2 O₂ observations. This work was made possible by grants from NSF Polar Programs
919 (1501993, 1501997, 1501292, 1502301, 1543457), NSF Atmospheric Chemistry Grants
920 1535364, 1623745, and 1623748 and NASA funding of the EVS2 Atmospheric Tomography
921 (ATom) project, as well as the support of the NCAR Advanced Study Program (ASP)
922 Postdoctoral Fellowship Program and computing support from Yellowstone, provided by
923 NCAR's Computational and Information Systems Laboratory. The National Center for
924 Atmospheric Research is sponsored by the National Science Foundation.

925

926 References

- 927 Abrahamsson, K., Lorén, A., Wulff, A. and Wängberg, S.-Å.: Air–sea exchange of halocarbons: the influence of
 928 diurnal and regional variations and distribution of pigments, *Deep Sea Research Part II: Topical Studies in*
 929 *Oceanography*, 51(22–24), 2789–2805, doi:10.1016/j.dsr2.2004.09.005, 2004a.
- 930 Abrahamsson, K., Bertilsson, S., Chierici, M., Fransson, A., Froneman, P. W., Lorén, A. and Pakhomov, E. A.:
 931 Variations of biochemical parameters along a transect in the Southern Ocean, with special emphasis on volatile
 932 halogenated organic compounds, *Deep Sea Research Part II: Topical Studies in Oceanography*, 51(22–24), 2745–
 933 2756, doi:10.1016/j.dsr2.2004.09.004, 2004b.
- 934 Abrahamsson, K., Granfors, A., Ahnoff, M., Cuevas, C. A. and Saiz-Lopez, A.: Organic bromine compounds
 935 produced in sea ice in Antarctic winter, *Nature Communications*, 9(1), doi:10.1038/s41467-018-07062-8, 2018.
- 936 Anav, A., Friedlingstein, P., Beer, C., Ciais, P., Harper, A., Jones, C., Murray-Tortarolo, G., Papale, D., Parazoo, N.
 937 C., Peylin, P., Piao, S., Sitch, S., Viovy, N., Wiltshire, A. and Zhao, M.: Spatiotemporal patterns of terrestrial gross
 938 primary production: A review: GPP Spatiotemporal Patterns, *Reviews of Geophysics*, 53(3), 785–818,
 939 doi:10.1002/2015RG000483, 2015.
- 940 Apel, E.: ORCAS Trace Organic Gas Analyzer (TOGA) VOC Data. Version 1.0, [online] Available from:
 941 <https://data.eol.ucar.edu/dataset/490.018> (Accessed 29 January 2019), 2017.
- 942 Apel, E. C., Hornbrook, R. S., Hills, A. J., Blake, N. J., Barth, M. C., Weinheimer, A., Cantrell, C., Rutledge, S. A.,
 943 Basarab, B., Crawford, J., Diskin, G., Homeyer, C. R., Campos, T., Flocke, F., Fried, A., Blake, D. R., Brune, W.,
 944 Pollack, I., Peischl, J., Ryerson, T., Wennberg, P. O., Crounse, J. D., Wisthaler, A., Mikoviny, T., Huey, G., Heikes,
 945 B., O’Sullivan, D. and Riemer, D. D.: Upper tropospheric ozone production from lightning NO_x-impacted
 946 convection: Smoke ingestion case study from the DC3 campaign, *Journal of Geophysical Research: Atmospheres*,
 947 120(6), 2505–2523, doi:10.1002/2014JD022121, 2015.
- 948 Atkinson, H. M., Huang, R.-J., Chance, R., Roscoe, H. K., Hughes, C., Davison, B., Schönhardt, A., Mahajan, A. S.,
 949 Saiz-Lopez, A., Hoffmann, T. and Liss, P. S.: Iodine emissions from the sea ice of the Weddell Sea, *Atmospheric*
 950 *Chemistry and Physics*, 12(22), 11229–11244, doi:10.5194/acp-12-11229-2012, 2012.
- 951 Atlas, E.: ORCAS Advanced Whole Air Sampler (AWAS) Data. Version 1.0, [online] Available from:
 952 <https://data.eol.ucar.edu/dataset/490.027> (Accessed 29 January 2019), 2017.
- 953 Ayers, G. P.: Comment on regression analysis of air quality data, *Atmospheric Environment*, 35(13), 2423–2425,
 954 doi:10.1016/S1352-2310(00)00527-6, 2001.
- 955 Bates, T. S.: Preface [to special section on First Aerosol Characterization Experiment (AGE 1)], *Journal of*
 956 *Geophysical Research: Atmospheres*, 104(D17), 21645–21647, doi:10.1029/1999JD900365, 1999.
- 957 Bell, N., Hsu, L., Jacob, D. J., Schultz, M. G., Blake, D. R., Butler, J. H., King, D. B., Lobert, J. M. and Maier-
 958 Reimer, E.: Methyl iodide: Atmospheric budget and use as a tracer of marine convection in global models:
 959 GLOBAL ATMOSPHERIC METHYL IODIDE, *Journal of Geophysical Research: Atmospheres*, 107(D17), ACH
 960 8–1–ACH 8–12, doi:10.1029/2001JD001151, 2002.
- 961 Blake, N. J., Blake, D. R., Wingenter, O. W., Sive, B. C., Kang, C. H., Thornton, D. C., Bandy, A. R., Atlas, E.,
 962 Flocke, F., Harris, J. M. and Rowland, F. S.: Aircraft measurements of the latitudinal, vertical, and seasonal
 963 variations of NMHCs, methyl nitrate, methyl halides, and DMS during the First Aerosol Characterization
 964 Experiment (ACE 1), *Journal of Geophysical Research: Atmospheres*, 104(D17), 21803–21817,
 965 doi:10.1029/1999JD900238, 1999.
- 966 Blei, E. and Heal, M. R.: Methyl bromide and methyl chloride fluxes from temperate forest litter, *Atmospheric*
 967 *Environment*, 45(8), 1543–1547, doi:10.1016/j.atmosenv.2010.12.044, 2011.
- 968 [Bloss, W. J., J. D. Lee, G. P. Johnson, R. Sommariva, D. E. Heard, A. Saiz-Lopez, J. M. C. Plane, G. McFiggans,](#)
 969 [M. Flynn, P. Williams, A. R. Rickard and Z. L. Fleming: Impact of halogen monoxide chemistry upon boundary](#)
 970 [layer OH and HO₂ concentrations at a coastal site, *Geophysical Research Letters*, 32\(6\),](#)
 971 [doi:10.1029/2004GL022084, 2005.](#)

972 |

973 Boden, T., Andres, R. and Marland, G.: Global, Regional, and National Fossil-Fuel CO₂ Emissions (1751 - 2014)
 974 (V. 2017), [online] Available from: <https://www.osti.gov/servlets/purl/1389331/> (Accessed 25 November 2018),
 975 2017.

976 Boucher, O., Moulin, C., Belviso, S., Aumont, O., Bopp, L., Cosme, E., von Kuhlmann, R., Lawrence, M. G., Pham,
 977 M., Reddy, M. S., Sciare, J. and Venkataraman, C.: DMS atmospheric concentrations and sulphate aerosol indirect
 978 radiative forcing: a sensitivity study to the DMS source representation and oxidation, *Atmospheric Chemistry and*
 979 *Physics*, 3(1), 49–65, doi:10.5194/acp-3-49-2003, 2003.

980 Butler, J. H., King, D. B., Lobert, J. M., Montzka, S. A., Yvon-Lewis, S. A., Hall, B. D., Warwick, N. J., Mondeel,
 981 D. J., Aydin, M. and Elkins, J. W.: Oceanic distributions and emissions of short-lived halocarbons: OCEANIC
 982 EMISSIONS OF SHORT-LIVED HALOCARBONS, *Global Biogeochemical Cycles*, 21(1),
 983 doi:10.1029/2006GB002732, 2007.

984 Cantrell, C. A.: Technical Note: Review of methods for linear least-squares fitting of data and application to
 985 atmospheric chemistry problems, *Atmospheric Chemistry and Physics*, 8(17), 5477–5487, doi:10.5194/acp-8-5477-
 986 2008, 2008.

987 Carpenter, L. J., Liss, P. S. and Penkett, S. A.: Marine organohalogens in the atmosphere over the Atlantic and
 988 Southern Oceans: MARINE ORGANOHALOGENS IN THE ATMOSPHERE, *Journal of Geophysical Research:*
 989 *Atmospheres*, 108(D9), n/a–n/a, doi:10.1029/2002JD002769, 2003.

990 Carpenter, L. J., Wevill, D. J., Palmer, C. J. and Michels, J.: Depth profiles of volatile iodine and bromine-
 991 containing halocarbons in coastal Antarctic waters, *Marine Chemistry*, 103(3-4), 227–236,
 992 doi:10.1016/j.marchem.2006.08.003, 2007.

993 Carpenter, L. J., Jones, C. E., Dunk, R. M., Hornsby, K. E. and Woeltjen, J.: Air-sea fluxes of biogenic bromine
 994 from the tropical and North Atlantic Ocean, *Atmospheric Chemistry and Physics*, 9(5), 1805–1816,
 995 doi:10.5194/acp-9-1805-2009, 2009.

996 Chuck, A. L.: Oceanic distributions and air-sea fluxes of biogenic halocarbons in the open ocean, *Journal of*
 997 *Geophysical Research*, 110(C10), doi:10.1029/2004JC002741, 2005.

998 Colomb, A., Yassaa, N., Williams, J., Peeken, I. and Lochte, K.: Screening volatile organic compounds (VOCs)
 999 emissions from five marine phytoplankton species by head space gas chromatography/mass spectrometry (HS-
 1000 GC/MS), *Journal of Environmental Monitoring*, 10(3), 325, doi:10.1039/b715312k, 2008.

1001 Drewer, J., Heal, K. V., Smith, K. A. and Heal, M. R.: Methyl bromide emissions to the atmosphere from temperate
 1002 woodland ecosystems, *Global Change Biology*, doi:10.1111/j.1365-2486.2008.01676.x, 2008.

1003 Emmons, L. K., Walters, S., Hess, P. G., Lamarque, J.-F., Pfister, G. G., Fillmore, D., Granier, C., Guenther, A.,
 1004 Kinnison, D., Laepple, T., Orlando, J., Tie, X., Tyndall, G., Wiedinmyer, C., Baughcum, S. L. and Kloster, S.:
 1005 Description and evaluation of the Model for Ozone and Related chemical Tracers, version 4 (MOZART-4),
 1006 *Geoscientific Model Development*, 3(1), 43–67, doi:10.5194/gmd-3-43-2010, 2010.

1007 Fernandez, R. P., Salawitch, R. J., Kinnison, D. E., Lamarque, J.-F. and Saiz-Lopez, A.: Bromine partitioning in the
 1008 tropical tropopause layer: implications for stratospheric injection, *Atmospheric Chemistry and Physics*, 14(24),
 1009 13391–13410, doi:10.5194/acp-14-13391-2014, 2014.

1010 Finlayson-Pitts, B. J.: The Tropospheric Chemistry of Sea Salt: A Molecular-Level View of the Chemistry of NaCl
 1011 and NaBr, *Chemical Reviews*, 103(12), 4801–4822, doi:10.1021/cr020653t, 2003.

1012 Garcia, H. E. and Keeling, R. F.: On the global oxygen anomaly and air-sea flux, *Journal of Geophysical Research:*
 1013 *Oceans*, 106(C12), 31155–31166, doi:10.1029/1999JC000200, 2001.

1014 Gent, P. R., Danabasoglu, G., Donner, L. J., Holland, M. M., Hunke, E. C., Jayne, S. R., Lawrence, D. M., Neale, R.
 1015 B., Rasch, P. J., Vertenstein, M., Worley, P. H., Yang, Z.-L. and Zhang, M.: The Community Climate System Model
 1016 Version 4, *Journal of Climate*, 24(19), 4973–4991, doi:10.1175/2011JCLI4083.1, 2011.

Elizabeth Asher 8/4/2019 2:02 PM

Deleted: Bloss, W. J.: Impact of halogen monoxide chemistry upon boundary layer OH and HO₂ concentrations at a coastal site, *Geophysical Research Letters*, 32(6), doi:10.1029/2004GL022084, 2005.

1022 von Glasow, R. and Crutzen, P. J.: Model study of multiphase DMS oxidation with a focus on halogens,
 1023 Atmospheric Chemistry and Physics, 4(3), 589–608, doi:10.5194/acp-4-589-2004, 2004.

1024 von Glasow, R., von Kuhlmann, R., Lawrence, M. G., Platt, U. and Crutzen, P. J.: Impact of reactive bromine
 1025 chemistry in the troposphere, Atmospheric Chemistry and Physics, 4(11/12), 2481–2497, doi:10.5194/acp-4-2481-
 1026 2004, 2004.

1027 Glover, D. M., Jenkins, W. J. and Doney, S. C.: Modeling Methods for Marine Science, Cambridge University
 1028 Press., 2011.

1029 Guenther, A. B., Jiang, X., Heald, C. L., Sakulyanontvittaya, T., Duhl, T., Emmons, L. K. and Wang, X.: The Model
 1030 of Emissions of Gases and Aerosols from Nature version 2.1 (MEGAN2.1): an extended and updated framework for
 1031 modeling biogenic emissions, Geoscientific Model Development, 5(6), 1471–1492, doi:10.5194/gmd-5-1471-2012,
 1032 2012.

1033 Happell, J. D., Wallace, D. W. R., Wills, K. D., Wilke, R. J. and Neill, C. C.: A purge-and-trap capillary column gas
 1034 chromatographic method for the measurement of halocarbons in water and air. [online] Available from:
 1035 <http://www.osti.gov/servlets/purl/366493-84sOfy/webviewable/> (Accessed 26 July 2018), 1996.

1036 Hossaini, R., Mantle, H., Chipperfield, M. P., Montzka, S. A., Hamer, P., Ziska, F., Quack, B., Krüger, K.,
 1037 Tegtmeier, S., Atlas, E., Sala, S., Engel, A., Bönisch, H., Keber, T., Oram, D., Mills, G., Ordóñez, C., Saiz-Lopez,
 1038 A., Warwick, N., Liang, Q., Feng, W., Moore, F., Miller, B. R., Marécal, V., Richards, N. A. D., Dorf, M. and
 1039 Pfeilsticker, K.: Evaluating global emission inventories of biogenic bromocarbons, Atmospheric Chemistry and
 1040 Physics, 13(23), 11819–11838, doi:10.5194/acp-13-11819-2013, 2013.

1041 Hughes, C., Chuck, A. L., Rossetti, H., Mann, P. J., Turner, S. M., Clarke, A., Chance, R. and Liss, P. S.: Seasonal
 1042 cycle of seawater bromoform and dibromomethane concentrations in a coastal bay on the western Antarctic
 1043 Peninsula: BROMOCARBON SEASONALITY ANTARCTICA, Global Biogeochemical Cycles, 23(2), n/a–n/a,
 1044 doi:10.1029/2008GB003268, 2009.

1045 Hughes, C., Johnson, M., Utting, R., Turner, S., Malin, G., Clarke, A. and Liss, P. S.: Microbial control of
 1046 bromocarbon concentrations in coastal waters of the western Antarctic Peninsula, Marine Chemistry, 151, 35–46,
 1047 doi:10.1016/j.marchem.2013.01.007, 2013.

1048 Hurrell, J. W., Hack, J. J., Shea, D., Caron, J. M. and Rosinski, J.: A New Sea Surface Temperature and Sea Ice
 1049 Boundary Dataset for the Community Atmosphere Model, Journal of Climate, 21(19), 5145–5153,
 1050 doi:10.1175/2008JCLI2292.1, 2008.

1051 Keeling, R. F., Manning, A. C., McEvoy, E. M. and Shertz, S. R.: Methods for measuring changes in atmospheric O
 1052 ₂ concentration and their application in southern hemisphere air, Journal of Geophysical Research: Atmospheres,
 1053 103(D3), 3381–3397, doi:10.1029/97JD02537, 1998.

1054 Lai, S. C., Williams, J., Arnold, S. R., Atlas, E. L., Gebhardt, S. and Hoffmann, T.: Iodine containing species in the
 1055 remote marine boundary layer: A link to oceanic phytoplankton: IODINE SPECIES AND PHYTOPLANKTON,
 1056 Geophysical Research Letters, 38(20), n/a–n/a, doi:10.1029/2011GL049035, 2011.

1057 Lamarque, J.-F.: Response of a coupled chemistry-climate model to changes in aerosol emissions: Global impact on
 1058 the hydrological cycle and the tropospheric burdens of OH, ozone, and NO_x, Geophysical Research Letters, 32(16),
 1059 doi:10.1029/2005GL023419, 2005.

1060 Lamarque, J.-F., Emmons, L. K., Hess, P. G., Kinnison, D. E., Tilmes, S., Vitt, F., Heald, C. L., Holland, E. A.,
 1061 Lauritzen, P. H., Neu, J., Orlando, J. J., Rasch, P. J. and Tyndall, G. K.: CAM-chem: description and evaluation of
 1062 interactive atmospheric chemistry in the Community Earth System Model, Geoscientific Model Development, 5(2),
 1063 369–411, doi:10.5194/gmd-5-369-2012, 2012.

1064 Laturnus, F.: Volatile halocarbons released from Arctic macroalgae, Marine Chemistry, 55(3-4), 359–366,
 1065 doi:10.1016/S0304-4203(97)89401-7, 1996.

1066 Liang, Q., Atlas, E., Blake, D., Dorf, M., Pfeilsticker, K. and Schauffler, S.: Convective transport of very short lived
1067 bromocarbons to the stratosphere, *Atmospheric Chemistry and Physics*, 14(11), 5781–5792, doi:10.5194/acp-14-
1068 5781-2014, 2014.

1069 Lin, J. C.: A near-field tool for simulating the upstream influence of atmospheric observations: The Stochastic Time-
1070 Inverted Lagrangian Transport (STILT) model, *Journal of Geophysical Research*, 108(D16), ACH 2–1–ACH 2–17,
1071 doi:10.1029/2002JD003161, 2003.

1072 Liu, X., Easter, R. C., Ghan, S. J., Zaveri, R., Rasch, P., Shi, X., Lamarque, J.-F., Gettelman, A., Morrison, H., Vitt,
1073 F., Conley, A., Park, S., Neale, R., Hannay, C., Ekman, A. M. L., Hess, P., Mahowald, N., Collins, W., Iacono, M.
1074 J., Bretherton, C. S., Flanner, M. G. and Mitchell, D.: Toward a minimal representation of aerosols in climate
1075 models: description and evaluation in the Community Atmosphere Model CAM5, *Geoscientific Model*
1076 *Development*, 5(3), 709–739, doi:10.5194/gmd-5-709-2012, 2012.

1077 Manley, S. L. and Dastoor, M. N.: Methyl iodide (CH₃I) production by kelp and associated microbes, *Marine*
1078 *Biology*, 98(4), 477–482, doi:10.1007/BF00391538, 1988.

1079 Maslanik, J.: Near-Real-Time DMSP SSM/I-SSMIS Daily Polar Gridded Sea Ice Concentrations, Version 1, 1999.

1080 Mattson, E., Karlsson, A., Smith, W. O. and Abrahamsson, K.: The relationship between biophysical variables and
1081 halocarbon distributions in the waters of the Amundsen and Ross Seas, Antarctica, *Marine Chemistry*, 140–141, 1–9,
1082 doi:10.1016/j.marchem.2012.07.002, 2012.

1083 Mattsson, E., Karlsson, A. and Abrahamsson, K.: Regional sinks of bromoform in the Southern Ocean: REGIONAL
1084 SINKS OF CHBR₃ IN THE ANTARCTIC, *Geophysical Research Letters*, 40(15), 3991–3996,
1085 doi:10.1002/grl.50783, 2013.

1086 Moore, R. M. and Groszko, W.: Methyl iodide distribution in the ocean and fluxes to the atmosphere, *Journal of*
1087 *Geophysical Research: Oceans*, 104(C5), 11163–11171, doi:10.1029/1998JC900073, 1999.

1088 Moore, R. M. and Zafiriou, O. C.: Photochemical production of methyl iodide in seawater, *Journal of Geophysical*
1089 *Research*, 99(D8), 16415, doi:10.1029/94JD00786, 1994.

1090 Moore, R. M., Webb, M., Tokarczyk, R. and Wever, R.: Bromoperoxidase and iodoperoxidase enzymes and
1091 production of halogenated methanes in marine diatom cultures, *Journal of Geophysical Research: Oceans*, 101(C9),
1092 20899–20908, doi:10.1029/96JC01248, 1996.

1093 Murphy, D. M., Froyd, K. D., Bian, H., Brock, C. A., Dibb, J. E., DiGangi, J. P., Diskin, G., Dollner, M., Kupc, A.,
1094 Scheuer, E. M., Schill, G. P., Weinzierl, B., Williamson, C. J. and Yu, P.: The distribution of sea-salt aerosol in the
1095 global troposphere, *Atmospheric Chemistry and Physics Discussions*, 1–27, doi:10.5194/acp-2018-1013, 2018.

1096 NASA Goddard Space Flight Center, O. E. L.: SeaWiFS Ocean Color Data, 2014.

1097 National Centers For Environmental Prediction/National Weather Service/NOAA/U.S. Department Of Commerce:
1098 NCEP GDAS/FNL 0.25 Degree Global Tropospheric Analyses and Forecast Grids, 2015.

1099 Navarro, M. A., Atlas, E. L., Saiz-Lopez, A., Rodriguez-Lloveras, X., Kinnison, D. E., Lamarque, J.-F., Tilmes, S.,
1100 Filus, M., Harris, N. R. P., Meneguz, E., Ashfold, M. J., Manning, A. J., Cuevas, C. A., Schauffler, S. M. and
1101 Donets, V.: Airborne measurements of organic bromine compounds in the Pacific tropical tropopause layer,
1102 *Proceedings of the National Academy of Sciences*, 112(45), 13789–13793, doi:10.1073/pnas.1511463112, 2015.

1103 Neale, R. B., Richter, J., Park, S., Lauritzen, P. H., Vavrus, S. J., Rasch, P. J. and Zhang, M.: The Mean Climate of
1104 the Community Atmosphere Model (CAM4) in Forced SST and Fully Coupled Experiments, *Journal of Climate*,
1105 26(14), 5150–5168, doi:10.1175/JCLI-D-12-00236.1, 2013.

1106 Nevison, C. D., Manizza, M., Keeling, R. F., Kahru, M., Bopp, L., Dunne, J., Tiputra, J., Ilyina, T. and Mitchell, B.
1107 G.: Evaluating the ocean biogeochemical components of Earth system models using atmospheric potential oxygen
1108 and ocean color data, *Biogeosciences*, 12(1), 193–208, doi:10.5194/bg-12-193-2015, 2015.

1109 Nevison, C. D., Manizza, M., Keeling, R. F., Stephens, B. B., Bent, J. D., Dunne, J., Ilyina, T., Long, M.,
1110 Resplandy, L., Tjiputra, J. and Yukimoto, S.: Evaluating CMIP5 ocean biogeochemistry and Southern Ocean carbon

1111 uptake using atmospheric potential oxygen: Present-day performance and future projection: CMIP5 APO AND
 1112 SOUTHERN OCEAN CARBON FLUX, *Geophysical Research Letters*, 43(5), 2077–2085,
 1113 doi:10.1002/2015GL067584, 2016.

1114 Nightingale, P. D., Malin, G. and Liss, P. S.: Production of chloroform and other low molecular-weight halocarbons
 1115 by some species of macroalgae, *Limnology and Oceanography*, 40(4), 680–689, doi:10.4319/lo.1995.40.4.0680,
 1116 1995.

1117 Nightingale, P. D., Malin, G., Law, C. S., Watson, A. J., Liss, P. S., Liddicoat, M. I., Boutin, J. and Upstill-Goddard,
 1118 R. C.: In situ evaluation of air-sea gas exchange parameterizations using novel conservative and volatile tracers,
 1119 *Global Biogeochemical Cycles*, 14(1), 373–387, 2000.

1120 Obrist, D., Tas, E., Peleg, M., Matveev, V., Faïn, X., Asaf, D. and Luria, M.: Bromine-induced oxidation of mercury
 1121 in the mid-latitude atmosphere, *Nature Geoscience*, 4, 22, 2010.

1122 Ordóñez, C., Lamarque, J.-F., Tilmes, S., Kinnison, D. E., Atlas, E. L., Blake, D. R., Sousa Santos, G., Brasseur, G.
 1123 and Saiz-Lopez, A.: Bromine and iodine chemistry in a global chemistry-climate model: description and evaluation
 1124 of very short-lived oceanic sources, *Atmospheric Chemistry and Physics*, 12(3), 1423–1447, doi:10.5194/acp-12-
 1125 1423-2012, 2012.

1126 Quack, B. and Wallace, D. W. R.: Air-sea flux of bromoform: Controls, rates, and implications: AIR-SEA FLUX
 1127 OF BROMOFORM, *Global Biogeochemical Cycles*, 17(1), doi:10.1029/2002GB001890, 2003.

1128 Raimund, S., Quack, B., Bozec, Y., Vernet, M., Rossi, V., Garçon, V., Morel, Y. and Morin, P.: Sources of short-
 1129 lived bromocarbons in the Iberian upwelling system, *Biogeosciences*, 8(6), 1551–1564, doi:10.5194/bg-8-1551-
 1130 2011, 2011.

1131 Read, K. A., Mahajan, A. S., Carpenter, L. J., Evans, M. J., Faria, B. V. E., Heard, D. E., Hopkins, J. R., Lee, J. D.,
 1132 Moller, S. J., Lewis, A. C., Mendes, L., McQuaid, J. B., Oetjen, H., Saiz-Lopez, A., Pilling, M. J. and Plane, J. M.
 1133 C.: Extensive halogen-mediated ozone destruction over the tropical Atlantic Ocean, *Nature*, 453(7199), 1232–1235,
 1134 doi:10.1038/nature07035, 2008.

1135 Resplandy, L., Keeling, R. F., Stephens, B. B., Bent, J. D., Jacobson, A., Rödenbeck, C. and Khatiwala, S.:
 1136 Constraints on oceanic meridional heat transport from combined measurements of oxygen and carbon, *Climate*
 1137 *Dynamics*, 47(9–10), 3335–3357, doi:10.1007/s00382-016-3029-3, 2016.

1138 Reygondeau, G., Longhurst, A., Martinez, E., Beaugrand, G., Antoine, D. and Maury, O.: Dynamic biogeochemical
 1139 provinces in the global ocean: DYNAMIC BIOGEOCHEMICAL PROVINCES, *Global Biogeochemical Cycles*,
 1140 27(4), 1046–1058, doi:10.1002/gbc.20089, 2013.

1141 Richter, U. and Wallace, D. W. R.: Production of methyl iodide in the tropical Atlantic Ocean: PRODUCTION OF
 1142 METHYL IODIDE, *Geophysical Research Letters*, 31(23), doi:10.1029/2004GL020779, 2004.

1143 Rienecker, M. M., Suarez, M. J., Todling, R., Bacmeister, J., Takacs, L., Liu, H. C., Gu, W., Sienkiewicz, M.,
 1144 Koster, R. D., Gelaro, R., Stajner, I. and Nielsen, J. E.: The GEOS-5 Data Assimilation System – Documentation of
 1145 Versions 5.0.1, 5.1.0, and 5.2.0, NASA/TM-2008-104606., 2008.

1146 Saiz-Lopez, A., Mahajan, A. S., Salmon, R. A., Bauguutte, S. J.-B., Jones, A. E., Roscoe, H. K. and Plane, J. M. C.:
 1147 Boundary Layer Halogens in Coastal Antarctica, *Science*, 317(5836), 348–351, doi:10.1126/science.1141408, 2007.

1148 Saiz-Lopez, A., Lamarque, J.-F., Kinnison, D. E., Tilmes, S., Ordóñez, C., Orlando, J. J., Conley, A. J., Plane, J. M.
 1149 C., Mahajan, A. S., Sousa Santos, G., Atlas, E. L., Blake, D. R., Sander, S. P., Schauffler, S., Thompson, A. M. and
 1150 Brasseur, G.: Estimating the climate significance of halogen-driven ozone loss in the tropical marine troposphere,
 1151 *Atmospheric Chemistry and Physics*, 12(9), 3939–3949, doi:10.5194/acp-12-3939-2012, 2012.

1152 Saiz-Lopez, A., Fernandez, R. P., Ordóñez, C., Kinnison, D. E., Gómez Martín, J. C., Lamarque, J.-F. and Tilmes,
 1153 S.: Iodine chemistry in the troposphere and its effect on ozone, *Atmospheric Chemistry and Physics*, 14(23), 13119–
 1154 13143, doi:10.5194/acp-14-13119-2014, 2014.

1155 Salawitch, R. J., Canty, T., Kurosu, T., Chance, K., Liang, Q., da Silva, A., Pawson, S., Nielsen, J. E., Rodriguez, J.
 1156 M., Bhartia, P. K., Liu, X., Huey, L. G., Liao, J., Stickel, R. E., Tanner, D. J., Dibb, J. E., Simpson, W. R.,
 1157 Donohoue, D., Weinheimer, A., Flocke, F., Knapp, D., Montzka, D., Neuman, J. A., Nowak, J. B., Ryerson, T. B.,
 1158 Oltmans, S., Blake, D. R., Atlas, E. L., Kinnison, D. E., Tilmes, S., Pan, L. L., Hendrick, F., Van Roozendaal, M.,
 1159 Kreher, K., Johnston, P. V., Gao, R. S., Johnson, B., Bui, T. P., Chen, G., Pierce, R. B., Crawford, J. H. and Jacob,
 1160 D. J.: A new interpretation of total column BrO during Arctic spring: FRONTIER, Geophysical Research Letters,
 1161 37(21), n/a–n/a, doi:10.1029/2010GL043798, 2010.

1162 Schauffler, S. M., Atlas, E. L., Blake, D. R., Flocke, F., Lueb, R. A., Lee-Taylor, J. M., Stroud, V. and Travnicsek,
 1163 W.: Distributions of brominated organic compounds in the troposphere and lower stratosphere, Journal of
 1164 Geophysical Research: Atmospheres, 104(D17), 21513–21535, doi:10.1029/1999JD900197, 1999.

1165 Schroeder, W. H., Anlauf, K. G., Barrie, L. A., Lu, J. Y., Steffen, A., Schneeberger, D. R. and Berg, T.: Arctic
 1166 springtime depletion of mercury, Nature, 394, 331, 1998.

1167 Simpson, W. R., Brown, S. S., Saiz-Lopez, A., Thornton, J. A. and von Glasow, R.: Tropospheric Halogen
 1168 Chemistry: Sources, Cycling, and Impacts, Chemical Reviews, 115(10), 4035–4062, doi:10.1021/cr5006638, 2015.

1169 Sive, B. C., Varner, R. K., Mao, H., Blake, D. R., Wingenter, O. W. and Talbot, R.: A large terrestrial source of
 1170 methyl iodide, Geophysical Research Letters, 34(17), doi:10.1029/2007GL030528, 2007.

1171 Stephens, B.: ORCAS Merge Products. Version 1.0, [online] Available from:
 1172 <https://data.eol.ucar.edu/dataset/490.024> (Accessed 31 December 2018), 2017.

1173 Stephens, B. B., Keeling, R. F., Heimann, M., Six, K. D., Murnane, R. and Caldeira, K.: Testing global ocean
 1174 carbon cycle models using measurements of atmospheric O₂ and CO₂ concentration, Global Biogeochemical
 1175 Cycles, 12(2), 213–230, doi:10.1029/97GB03500, 1998.

1176 Stephens, B. B., Keeling, R. F. and Paplawsky, W. J.: Shipboard measurements of atmospheric oxygen using a
 1177 vacuum-ultraviolet absorption technique, Tellus B, 55(4), 857–878, doi:10.1046/j.1435-6935.2003.00075.x, 2003.

1178 Stephens, B. B., Long, M. C., Keeling, R. F., Kort, E. A., Sweeney, C., Apel, E. C., Atlas, E. L., Beaton, S., Bent, J.
 1179 D., Blake, N. J., Bresch, J. F., Casey, J., Daube, B. C., Diao, M., Diaz, E., Dierssen, H., Donets, V., Gao, B.-C.,
 1180 Gierach, M., Green, R., Haag, J., Hayman, M., Hills, A. J., Hoecker-Martínez, M. S., Honomichl, S. B., Hornbrook,
 1181 R. S., Jensen, J. B., Li, R.-R., McCubbin, I., McKain, K., Morgan, E. J., Nolte, S., Powers, J. G., Rainwater, B.,
 1182 Randolph, K., Reeves, M., Schauffler, S. M., Smith, K., Smith, M., Stith, J., Stossmeister, G., Toohey, D. W. and
 1183 Watt, A. S.: The O₂/N₂ Ratio and CO₂ Airborne Southern Ocean Study, Bulletin of the American Meteorological
 1184 Society, 99(2), 381–402, doi:10.1175/BAMS-D-16-0206.1, 2018.

1185 Sturges, W. T., Cota, G. F. and Buckley, P. T.: Bromoform emission from Arctic ice algae, Nature, 358, 660, 1992.

1186 Sturges, W. T., Cota, G. F. and Buckley, P. T.: Vertical profiles of bromoform in snow, sea ice, and seawater in the
 1187 Canadian Arctic, Journal of Geophysical Research: Oceans, 102(C11), 25073–25083, doi:10.1029/97JC01860,
 1188 1997.

1189 Tilmes, S., Lamarque, J.-F., Emmons, L. K., Kinnison, D. E., Marsh, D., Garcia, R. R., Smith, A. K., Neely, R. R.,
 1190 Conley, A., Vitt, F., Val Martin, M., Tanimoto, H., Simpson, I., Blake, D. R. and Blake, N.: Representation of the
 1191 Community Earth System Model (CESM1) CAM4-chem within the Chemistry-Climate Model Initiative (CCMI),
 1192 Geoscientific Model Development, 9(5), 1853–1890, doi:10.5194/gmd-9-1853-2016, 2016.

1193 Tohjima, Y.: Preparation of gravimetric standards for measurements of atmospheric oxygen and reevaluation of
 1194 atmospheric oxygen concentration, Journal of Geophysical Research, 110(D11), doi:10.1029/2004JD005595, 2005.

1195 Tokarczyk, R. and Moore, R. M.: Production of volatile organohalogens by phytoplankton cultures, Geophysical
 1196 Research Letters, 21(4), 285–288, doi:10.1029/94GL00009, 1994.

1197 Tortell, P. D. and Long, M. C.: Spatial and temporal variability of biogenic gases during the Southern Ocean spring
 1198 bloom, Geophysical Research Letters, 36(1), doi:10.1029/2008GL035819, 2009.

1199 Tortell, P. D., Asher, E. C., Ducklow, H. W., Goldman, J. A. L., Dacey, J. W. H., Grzyski, J. J., Young, J. N.,
1200 Kranz, S. A., Bernard, K. S. and Morel, F. M. M.: Metabolic balance of coastal Antarctic waters revealed by
1201 autonomous $p\text{CO}_2$ and $\Delta\text{O}_2/\text{Ar}$ measurements: metabolic balance of Antarctic waters, *Geophysical Research*
1202 *Letters*, 41(19), 6803–6810, doi:10.1002/2014GL061266, 2014.

1203 Williams, J., Gros, V., Atlas, E., Maciejczyk, K., Batsaikhan, A., Schöler, H. F., Forster, C., Quack, B., Yassaa, N.,
1204 Sander, R. and Van Dingenen, R.: Possible evidence for a connection between methyl iodide emissions and Saharan
1205 dust, *Journal of Geophysical Research*, 112(D7), doi:10.1029/2005JD006702, 2007.

1206 WMO (World Meteorological Organization): Scientific Assessment of Ozone Depletion: 2018, Global Ozone
1207 Research and Monitoring Project-Report, Geneva, Switzerland., 2018.

1208 Wofsy, S. C.: HIAPER Pole-to-Pole Observations (HIPPO): fine-grained, global-scale measurements of climatically
1209 important atmospheric gases and aerosols, *Philosophical Transactions of the Royal Society A: Mathematical,*
1210 *Physical and Engineering Sciences*, 369(1943), 2073–2086, doi:10.1098/rsta.2010.0313, 2011.

1211 Wofsy, S. C., Afshar, S., Allen, H. M., Apel, E., Asher, E. C., Barletta, B., Bent, J., Bian, H., Biggs, B. C., Blake, D.
1212 R., Blake, N., Bourgois, L., Brock, C. A., Brune, W. H., Budney, J. W., Bui, T. P., Butler, A., Campuzano-Jost, P.,
1213 Chang, C. S., Chin, M., Commane, R., Correa, G., Crounse, J. D., Cullis, P. D., Daube, B. C., Day, D. A., Dean-
1214 Day, J. M., Dibb, J. E., Digangi, J. P., Diskin, G. S., Dollner, M., Elkins, J. W., Erdesz, F., Fiore, A. M., Flynn, C.
1215 M., Froyd, K., Gesler, D. W., Hall, S. R., Hanisco, T. F., Hannun, R. A., Hills, A. J., Hints, E. J., Hoffmann, A.,
1216 Hornbrook, R. S., Huey, L. G., Hughes, S., Jimenez, J. L., Johnson, B. J., Katich, J. M., Keeling, R., Kim, M. J.,
1217 Kupc, A., Lait, L. R., Lamarque, J.-F., Liu, H. B., McKain, K., McLaughlin, R. J., Meinardi, S., Miller, D. O.,
1218 Montzka, S. A., Moore, F. L., Morgan, E. J., Murphy, D. M., Murray, L. T., Nault, B. A., Neuman, J. A., Newman,
1219 P. A., Nicely, J. M., Pan, X., Paplawsky, W., Peischl, J., Prather, M. J., Price, D. J., Ray, E., Reeves, J. M.,
1220 Richardson, M., Rollins, A. W., Rosenlof, K. H., Ryerson, T. B., Scheuer, E., Schill, G. P., Schroder, J. C., Schwarz,
1221 J. P., St.Clair, J. M., Steenrod, S. D., Stephens, B. B., Strode, S. A., Sweeney, C., Tanner, D., Teng, A. P., Thames,
1222 A. B., Thompson, C. R., Ullmann, K., Veres, P. R., Vizenor, N., Wagner, N. L., Watt, A., Weber, R., Weinzierl, B.,
1223 et al.: ATom: Merged Atmospheric Chemistry, Trace Gases, and Aerosols, [online] Available from:
1224 https://daac.ornl.gov/cgi-bin/dsviewer.pl?ds_id=1581 (Accessed 31 December 2018), 2018.

1225 Xiang, B., Miller, S. M., Kort, E. A., Santoni, G. W., Daube, B. C., Commane, R., Angevine, W. M., Ryerson, T. B.,
1226 Trainer, M. K., Andrews, A. E., Nehrkorn, T., Tian, H. and Wofsy, S. C.: Nitrous oxide (N_2O) emissions from
1227 California based on 2010 CalNex airborne measurements: California N_2O emissions, *Journal of Geophysical*
1228 *Research: Atmospheres*, 118(7), 2809–2820, doi:10.1002/jgrd.50189, 2013.

1229 Yang, B., Yang, G.-P., Lu, X.-L., Li, L. and He, Z.: Distributions and sources of volatile chlorocarbons and
1230 bromocarbons in the Yellow Sea and East China Sea, *Marine Pollution Bulletin*, 95(1), 491–502,
1231 doi:10.1016/j.marpolbul.2015.03.009, 2015.

1232 Yokouchi, Y., Nojiri, Y., Barrie, L. A., Toom-Sauntry, D. and Fujinuma, Y.: Atmospheric methyl iodide: High
1233 correlation with surface seawater temperature and its implications on the sea-to-air flux, *Journal of Geophysical*
1234 *Research: Atmospheres*, 106(D12), 12661–12668, doi:10.1029/2001JD900083, 2001.

1235 Yokouchi, Y., Hasebe, F., Fujiwara, M., Takashima, H., Shiotani, M., Nishi, N., Kanaya, Y., Hashimoto, S., Fraser,
1236 P., Toom-Sauntry, D., Mukai, H. and Nojiri, Y.: Correlations and emission ratios among bromoform,
1237 dibromochloromethane, and dibromomethane in the atmosphere, *Journal of Geophysical Research*, 110(D23),
1238 doi:10.1029/2005JD006303, 2005.

1239 Ziska, F., Quack, B., Abrahamsson, K., Archer, S. D., Atlas, E., Bell, T., Butler, J. H., Carpenter, L. J., Jones, C. E.,
1240 Harris, N. R. P., Hepach, H., Heumann, K. G., Hughes, C., Kuss, J., Krüger, K., Liss, P., Moore, R. M., Orlikowska,
1241 A., Raimund, S., Reeves, C. E., Reifenhäuser, W., Robinson, A. D., Schall, C., Tanhua, T., Tegtmeier, S., Turner,
1242 S., Wang, L., Wallace, D., Williams, J., Yamamoto, H., Yvon-Lewis, S. and Yokouchi, Y.: Global sea-to-air flux
1243 climatology for bromoform, dibromomethane and methyl iodide, *Atmospheric Chemistry and Physics*, 13(17),
1244 8915–8934, doi:10.5194/acp-13-8915-2013, 2013.

1245

1246

1247 **Tables**

1248 Table 1. Mean ± uncertainty (see Sect. 3.4.1 and 3.4.2 for details) HVOC emission estimates
1249 (pmol m⁻² hr⁻¹) in Region 1 and Region 2 calculated in this study (with method indicated below
1250 each value), from CAM-Chem (Ordoñez et al., 2012) and from several other modeling and ship-
1251 based observational studies.

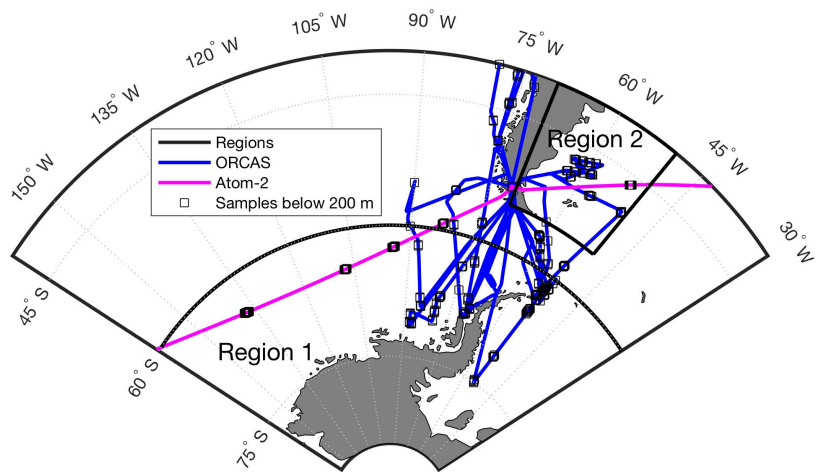
1252

Region/Months	CHBr ₃	CH ₂ Br ₂	CH ₃ I	CHClBr ₂	Reference
Region 1 (JF) <u><60° S</u>	91 ± 8 <u>O₂ Regr.</u>	31 ± 18 <u>O₂ Regr.</u>	35 ± 29 <u>MLR</u>	11 ± 4 <u>O₂ Regr.</u>	This Study
Region 2 (JF) <u>>55° S and</u> <u><40° S</u>	329 ± 23 <u>O₂ Regr.</u>	69 ± 5 <u>O₂ Regr.</u>	392 ± 32 <u>O₂ Regr.</u>	25 ± 5 <u>O₂ Regr.</u>	This Study
Region 1 (JF)	10	1.9	120	0.38	CAM-Chem
Region 2 (JF)	360	44	800	8.7	CAM-Chem
Southern Ocean (≥50°S), (DJ)	200	200	200	-----	Ziska et al. 2013 (model)
Marguerite Bay (DJF)	3500	875	-----	-----	Hughes et al. 2009 (obs)
70°S-72°S Antarctica	1300	-----	-----	-----	Carpenter et al. 2007 (obs)
Southern Ocean (≥50°S) (Feb. - April)	225	312	708	-----	Butler et al. 2007 (obs)
40°S-52°S S. Atlantic (Sept.- Feb.)	-1670	-----	250	-----	Chuck et al. 2005
Southern Ocean (≥50°S), (DJ)	-330	-----	-----	-----	Mattson et al. 2013 (model)

1253

1254

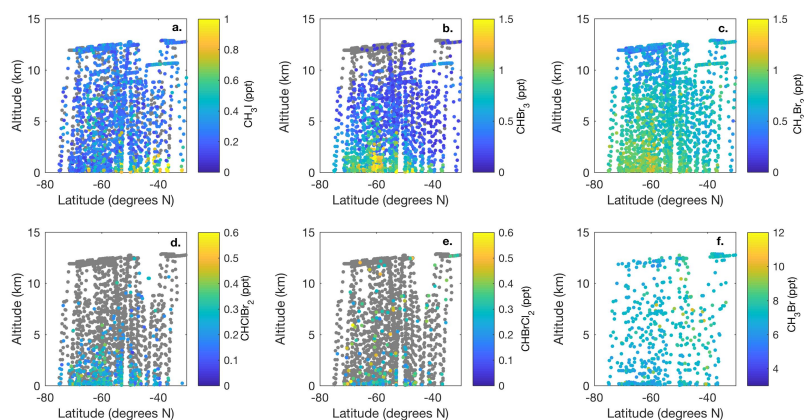
1255



1257
1258 **Figure 1.** Overview map ORCAS and ATom-2 flight tracks in the study regions: 1) high
1259 latitudes in the Southern Hemisphere poleward 60° S and 2) the Patagonian Shelf. The ORCAS
1260 and ATom-2 aircraft flights and dips below 200 m that took place within these regions are also
1261 shown.

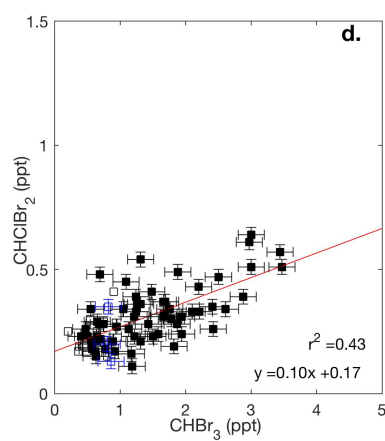
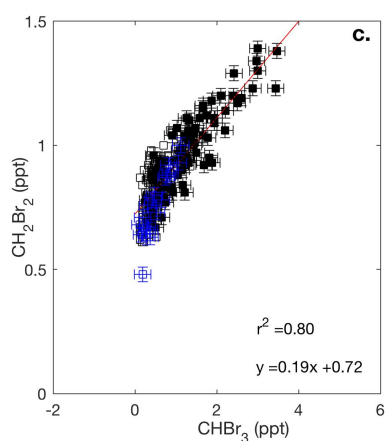
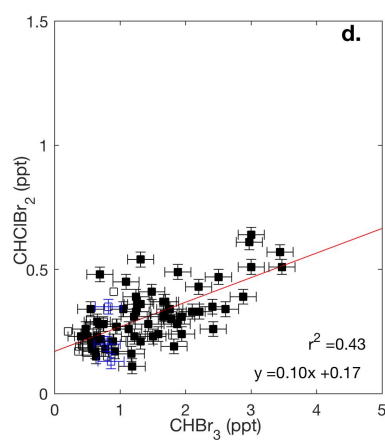
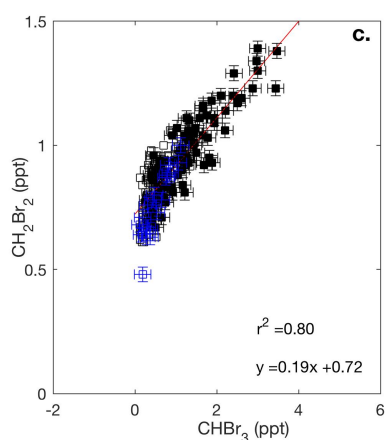
1262
1263

Unknown
Formatted: Font:(Default) Times, 12 pt,
Bold



Unknown
Formatted: Font:(Default) Times, 12 pt,
Bold

Figure 2. Meridional-altitudinal cross-sections of mixing ratios of a) CH_3I , b) CHBr_3 , c) CH_2Br_2 , d) CHClBr_2 , and e) CHBrCl_2 from the TOGA and mixing ratios of f) CH_3Br from AWAS and WAS in 2016 and 2017, respectively, during the ORCAS and ATom-2 campaigns over the Southern Ocean in the austral summer. Note the different color bar scales. Gray points denote measurements below the detection limit of each species ($\text{CH}_3\text{I} - 0.03 \text{ ppt}$, $\text{CHBr}_3 - 0.2 \text{ ppt}$, $\text{CH}_2\text{Br}_2 - 0.03 \text{ ppt}$, $\text{CHClBr}_2 - 0.03 \text{ ppt}$, $\text{CHBrCl}_2 - 0.05 \text{ ppt}$, $\text{CH}_3\text{Br} - 0.2 \text{ ppt}$).



Unknown
Formatted: Font:(Default) Times, 12 pt,
Bold

Figure 3. Mixing ratios of CHBr_3 vs. CH_2Br_2 and CHClBr_2 across the ORCAS and ATom-2 campaigns in Region 1 (Fig.3a,b) and in (Fig.3c,d), respectively. Type II major axis regression model (bivariate least squares regressions) are based on ORCAS data below 2 km and illustrate regional enhancement ratios. Error bars represent the uncertainty in HVOC measurements.

1283

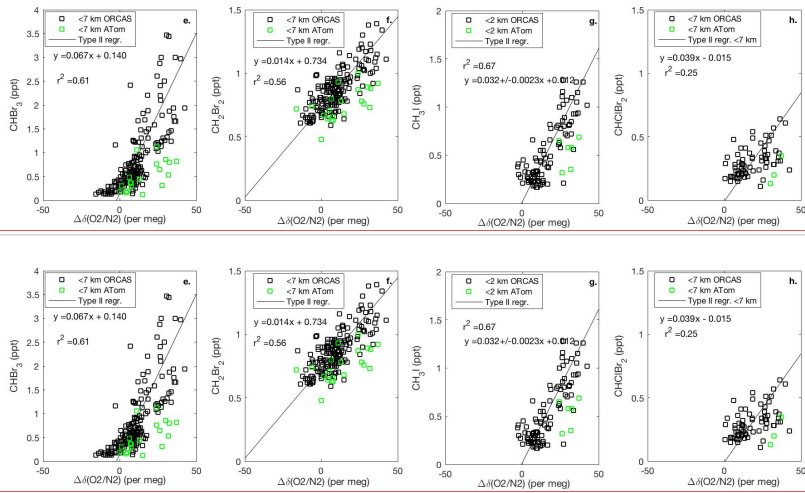
1284

1285

1286

1287 **Figure 4.** Mixing ratios of CHBr₃, CH₂Br₂, and CH₃I vs. O₂ on ORCAS and ATom-2 in Region
1288 1, poleward of 60° S (a-d) and Region 2 over the Patagonian Shelf (e-h). Slopes ± standard
1289 errors from type II major axis regression model (bivariate least squares regression) fits of
1290 ORCAS data for regressions with $r^2 > 0.2$ (fits were calculated on variables scaled to their full
1291 range). The slopes reported in the figure are converted to pmol:mol ratios prior to estimating
1292 biogenic HVOC fluxes based on modeled CESM O₂ fluxes. Data from above 7 km were
1293 excluded due to the influence of air masses transported from further north.

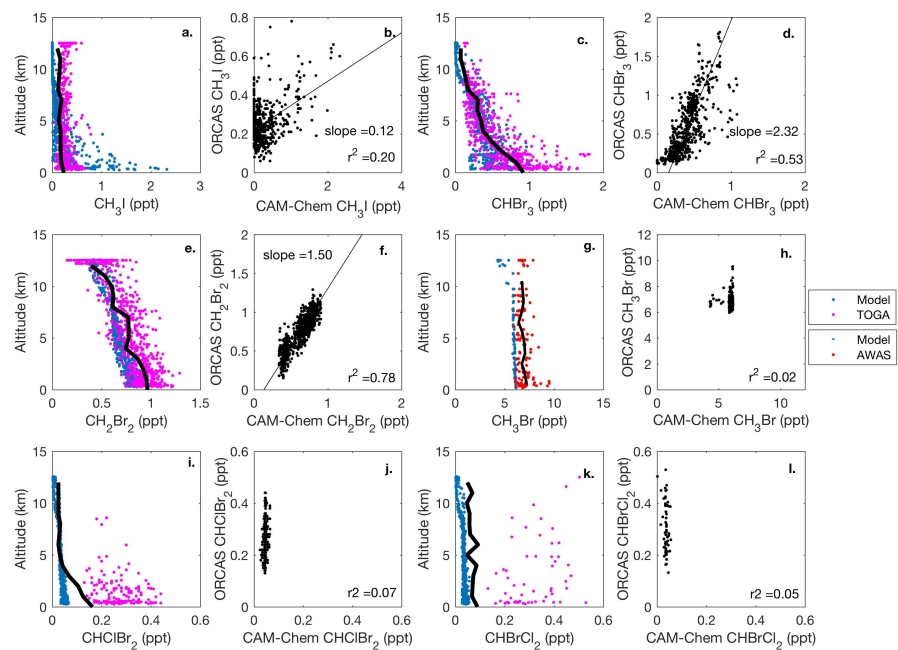
1294



Unknown
Formatted: Font:(Default) Times, 12 pt

Unknown
Formatted: Font:(Default) Times, 12 pt

1295
1296



1297

1298 **Fig 5.** CAM-Chem1.2 model-aircraft measurement comparison during the ORCAS campaign
1299 between 1-12 km in Region 1, high latitudes in the Southern Hemisphere poleward 60° S. All
1300 regressions are type II major axis regression models bivariate least squares regressions (slopes
1301 are shown when the $r^2 \geq 0.2$). The bold, black line in each vertical profile represents the binned
1302 (mean) mixing ratio of HVOC measurements at that altitude. The binned mean includes
1303 measurements below the detection limit (DL), which for this calculation are assigned a value
1304 equal to the DL multiplied by the percentage of data below detection. Modeled values include
1305 locations where observations were below the DL.

Unknown
Formatted: Font:(Default) Times, 12 pt

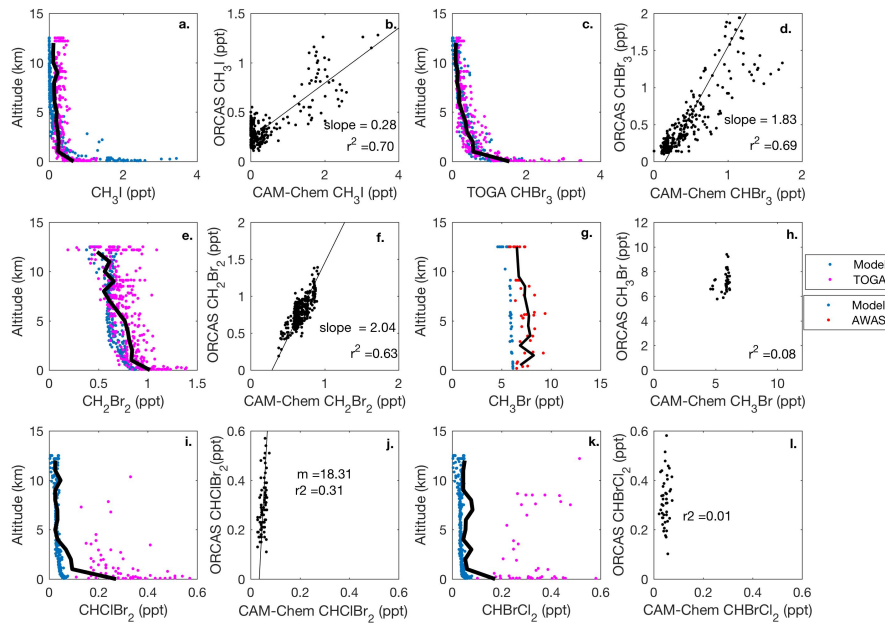


Figure 6. CAM-Chem 1.2 model-aircraft measurement (TOGA and AWAS) comparison during ORCAS campaign between 1-12 km in Region 2, the Patagonian Shelf. All regressions are type II major axis regression models bivariate least squares regressions (slopes are shown when the $r^2 \geq 0.2$). The bold, black line in each vertical profile represents the binned (mean) mixing ratio of HVOC measurements at that altitude. Again, the binned mean includes measurements below the detection limit (DL), which for this calculation are assigned a value equal to the DL multiplied by the percentage of data below detection. Modeled values include locations where observations were below the DL.

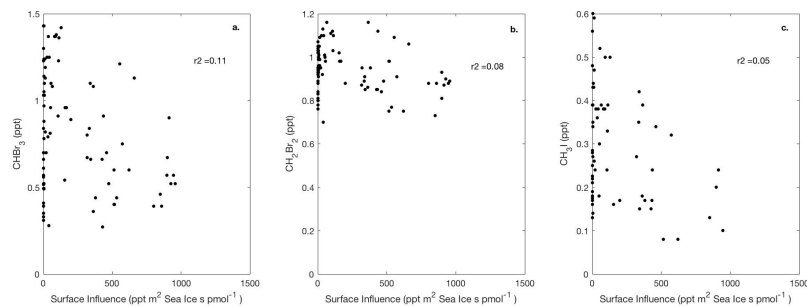


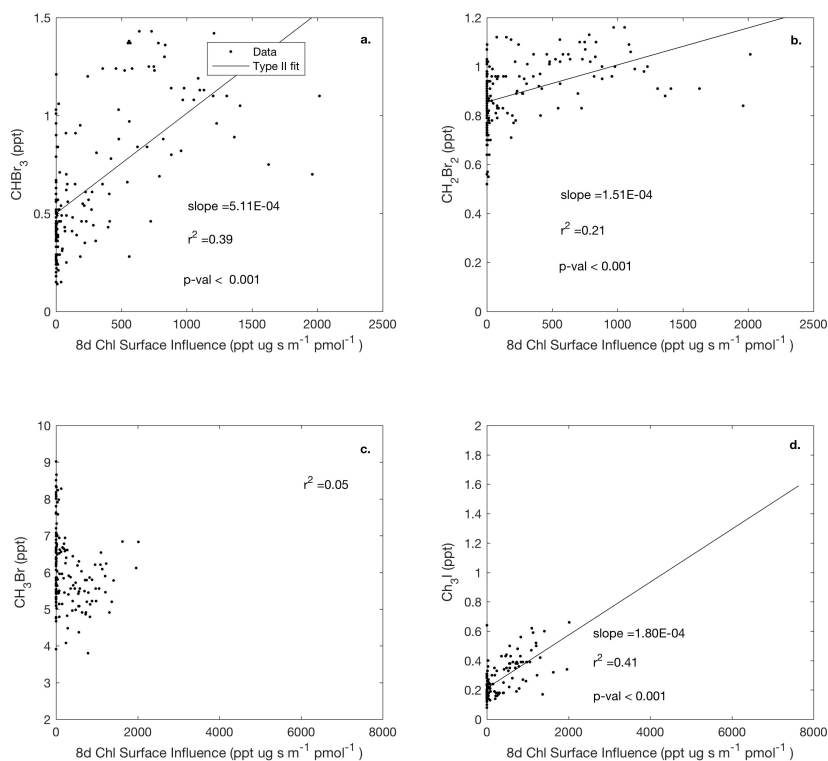
Figure 7. Linear type II regressions between influence functions convolved with sea ice distributions, which exclude land ice, and mixing ratios for CHBr_3 , CH_2Br_2 , and CH_3I in Region 1, poleward of 60° S . Surface influence ($\text{ppt m}^2 \text{ s pmol}^{-1}$) in each grid cell was multiplied by fractional sea ice concentration surface field, which is unit-less, yielding sea ice surface influence function units of $\text{ppt m}^2 \text{ s pmol}^{-1}$, as shown on the x-axis. Linear regression lines are not shown, as $p \geq 0.001$.

Unknown

Formatted: Font:(Default) Times, 12 pt

Elizabeth Asher 7/6/2019 11:31 AM

Deleted: predictor variable



Unknown

Formatted: Font:(Default) Times, 12 pt, Bold

1326

1327

1328 **Figure 8.** Linear type II regressions between influence functions of eight day composites of chl
 1329 *a* and mixing ratios of HVOCs (a-d) poleward of 60° S (Region 1). Surface influence (ppt m² s
 1330 pmol⁻¹) in each grid cell was multiplied by the chl *a* (μg m⁻³) surface field, resulting in surface
 1331 influence function units of μg ppt s pmol⁻¹ m⁻¹, shown on the x-axis. Linear regression lines are
 1332 shown where when $p < 0.001$.

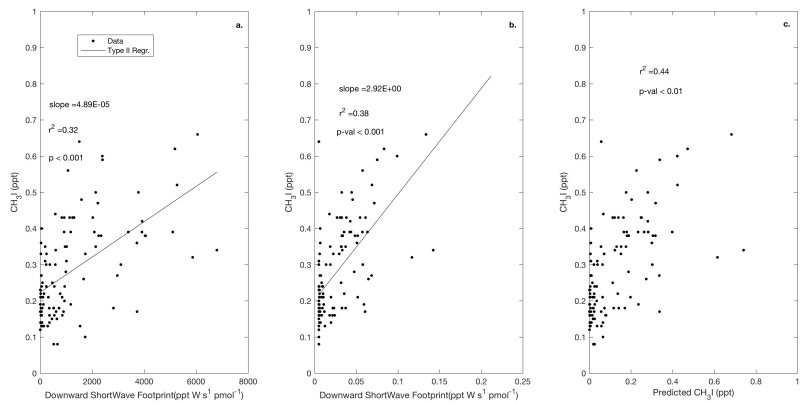
1333

Elizabeth Asher 7/6/2019 11:31 AM

Deleted: predictor variables

Elizabeth Asher 7/6/2019 10:26 AM

Deleted: .



1337

1338 **Figure 9.** Observed CH₃I plotted against the surface influence functions of downward shortwave
1339 radiation (a) and absorption due to detritus (b). Predicted mixing ratios of CH₃I based on a
1340 multiple linear regressions (MLR) using these two predictors in Region 1 are shown in Fig. 9c
1341 according to Equation 3. Surface influence (ppt m² s pmol⁻¹) in each grid cell was multiplied by
1342 the surface source field, such as shortwave radiation at the surface (W m⁻²), yielding units of ppt
1343 Ws pmol⁻¹, and the surface ocean's detrital absorption (m⁻¹), yielding units of ppt m s pmol⁻¹,
1344 shown on the x-axes.

1345

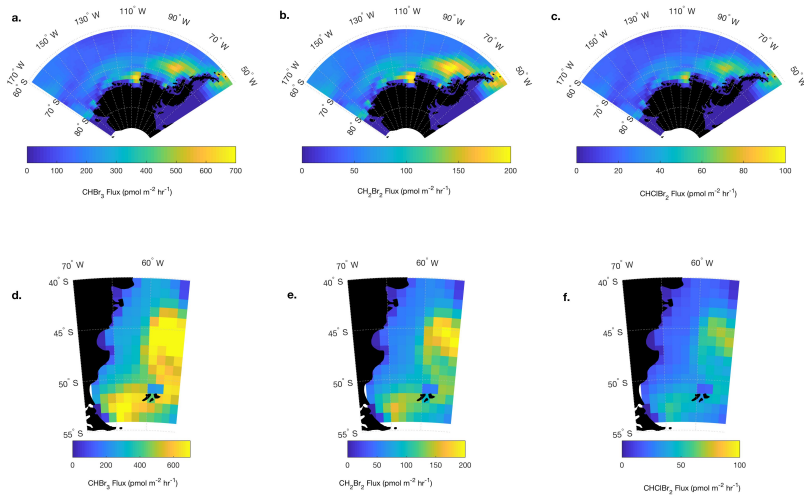
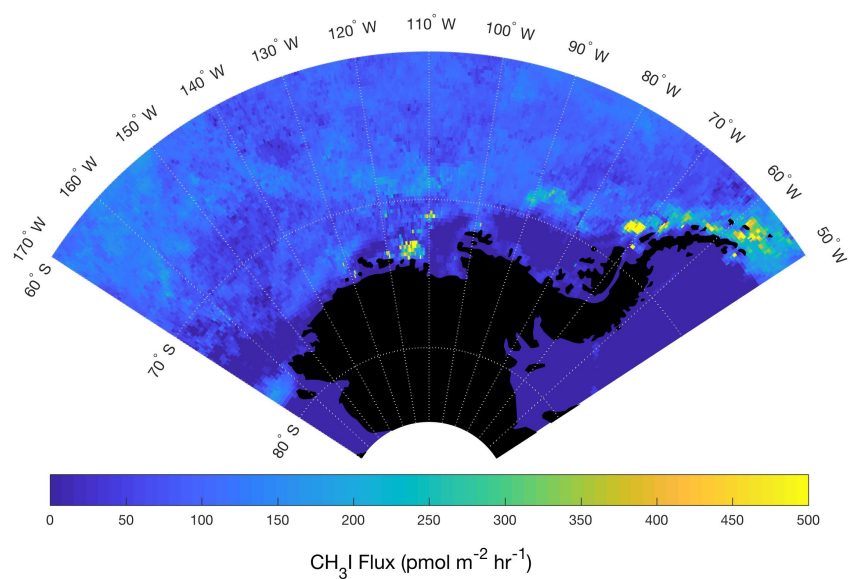


Figure 10. Resulting mean Jan. – Feb. 2016 O₂-based (parameterized) CHBr₃ and CH₂Br₂ and CHClBr₂ fluxes (pmol m⁻² s⁻¹) in Region 1 (a-c) poleward of 60° S and Region 2 (d-f) over the Patagonian Shelf. CESM modeled O₂ fluxes are scaled by the slope between the oceanic contribution to δ(O₂/N₂) and CHBr₃ and CH₂Br₂, and CHClBr₂ reported in Fig. 4. Note that these fluxes represent mean estimated biogenic fluxes in Jan. –Feb. 2016 (see Sect. 3.4.1 for details).

Unknown

Formatted: Font:(Default) Times, 12 pt



1353

1354 | **Figure 11.** Mean estimated CH₃I **fluxes** for Jan. – Feb. The multilinear regression in Fig. 9
 1355 between CH₃I mixing ratios and geophysical influence functions related to shortwave radiation
 1356 and detrital material at the sea surface was used to derive a mean flux field in Jan.-Feb., 2016 for
 1357 Region 1.

1358

1359 **Supplementary Text**

1360 **Sea-air exchange calculations**

1361 To support the interpretation of our results, we calculate nominal equilibration times. For
1362 estimates of bulk sea-air equilibration times for HVOCs, O₂, and CO₂, we assume a mixed layer
1363 depth of 30 m, a temperature of 0° C, a salinity of 35 PSU, and carbonate buffering according to
1364 eq. 8.3.10 in Sarmiento and Gruber (2006), and transfer velocities according to Nightingale et al.,
1365 (2000). The Schmidt number (i.e. the ratio of the kinematic viscosity of a gas, divided by the
1366 molecular diffusivity) for O₂, CO₂ and CH₃Br were calculated according to Wanninkhof (2014),
1367 and the Schmidt numbers for CHBr₃ and CH₃I were calculated according to Quack and Wallace
1368 (2003) and Moore and Groszko (1999), respectively. The results are provided in Sect. 3.1.2.

1369 **Comparisons of TOGA, WAS and PFP**

1370 Despite overall good agreement between co-located inflight AWAS, WAS, and PFP samples and
1371 TOGA measurements, we observed notable discrepancies in several cases (e.g. Fig. S1b; Fig.
1372 S2a-b). On ORCAS, we observed a non-linear relationship between inflight TOGA
1373 measurements and co-located AWAS samples of CH₃I (Fig. S1b), driven by a few samples with
1374 high mixing ratios. Close inspection of upwind and downwind flights over Region 2 with the
1375 campaign's high mixing ratios of CH₃I indicated that TOGA measurements were consistent with
1376 a modest flux of CH₃I from the ocean to the atmosphere. On ATom-2, TOGA measurements
1377 agreed better with co-located PFP samples than with co-located WAS samples; and differences
1378 on the sixth and seventh research flights (i.e. the data used here) were relatively small.
1379 Nevertheless these differences motivated an instrument inter-comparison following the ATom
1380 campaign between these instruments. Thus far, results of this inter-comparison show that TOGA
1381 and PFP measurements differ by < 25%.

1382

1383

1384 **Supplementary Tables**

1385 Table S1. The TOGA-PFP instrument comparison was done by sampling a 50L SS pontoon,
1386 created at NCAR from a humidified dilution of the TOGA ATom standard. Data were analyzed
1387 and reported by Rebecca Hornbrook (NCAR, TOGA) and Steve Montzka (NOAA, PFP).

Pontoon Inter-comparison	Concentration (dilution-based calc.)	TOGA (10/12/2018)	PFP (10/24/2018)
CHBr ₃	34	21.0 ± 0.1	26.6 ± 0.8
CHClBr ₂	26	19.9 ± 1.0	22.9 ± 0.1
CH ₂ Br ₂	52	47.7 ± 0.2	51.7 ± 2.0

1388

1389

Elizabeth Asher 7/8/2019 3:47 PM
Deleted: -

Elizabeth Asher 7/8/2019 3:48 PM
Deleted: -

Elizabeth Asher 7/7/2019 12:41 PM
Deleted: ,

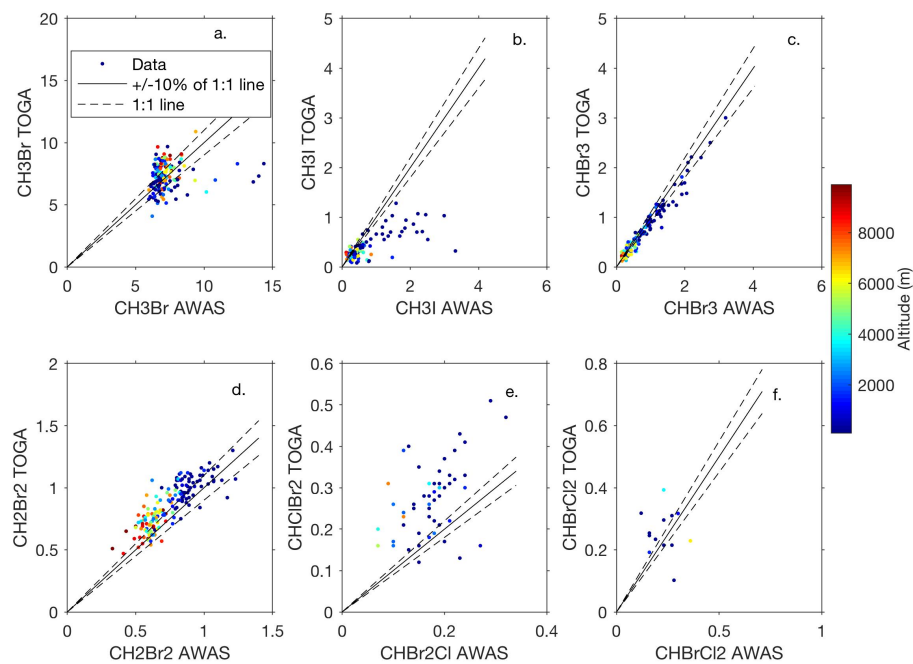
Elizabeth Asher 7/7/2019 12:41 PM
Formatted: Subscript

Elizabeth Asher 7/7/2019 12:41 PM
Formatted: Subscript

Elizabeth Asher 7/7/2019 12:41 PM
Formatted: Subscript

Elizabeth Asher 7/7/2019 12:41 PM
Formatted: Subscript

1393
1394 **Supplementary Figures**
1395



1396
1397
1398 **Figure S1.** Comparison between AWAS samples and TOGA measurements during ORCAS
1399 below 10 km, when these two shared over half their sampling period. Points are colored by
1400 altitude. Dashed lines represent $\pm 10\%$ of the 1:1 line. Sample points below the DL are not
1401 included in this quantitative comparison.

1402
1403

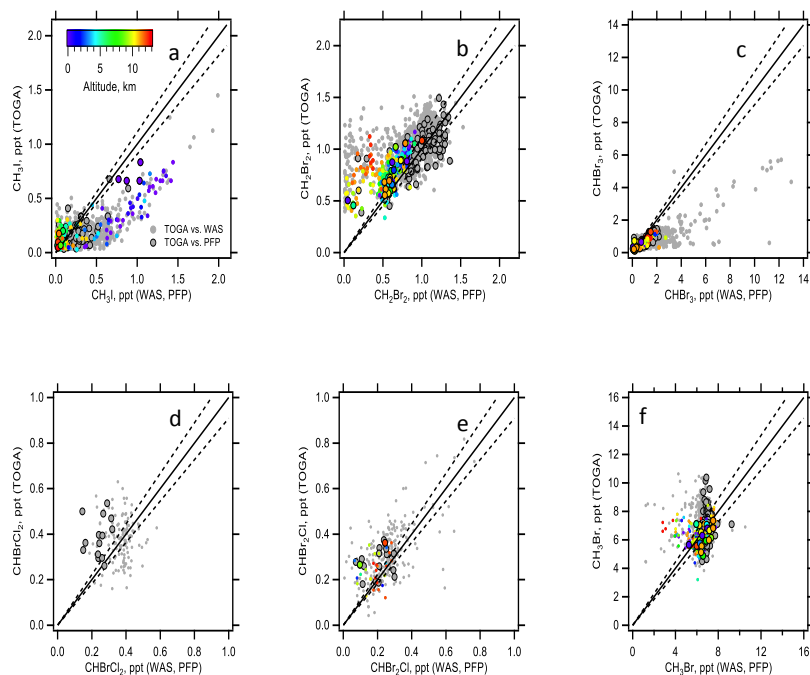


Figure S2. Comparison between WAS, PFP and TOGA measurements during ATom-2 below 10 km, when these instruments shared over half their sampling period. WAS measurements are shown in larger circles, PFP measurements in smaller circles, and measurements from the research flights six and seven used in this analysis are shown in color, while measurements on other research flights in ATom-2 are shown in gray. Dashed lines represent $\pm 10\%$ of the 1:1 line. Sample points below the DL are not shown.

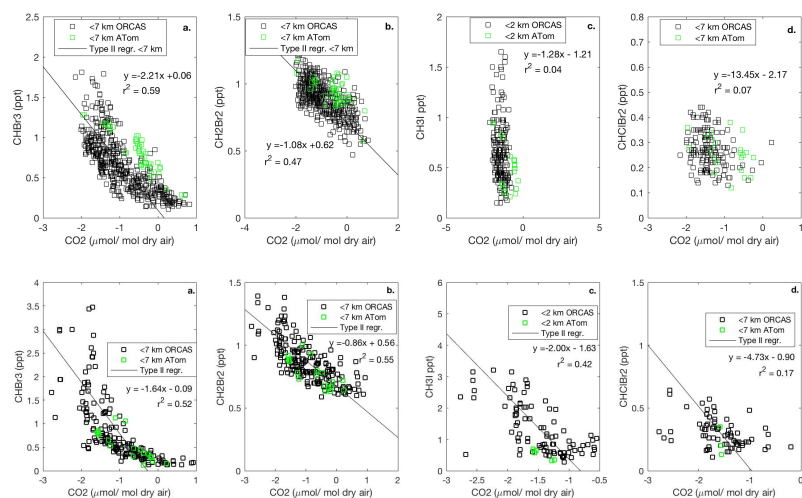


Figure S3. Mixing ratios of CHBr₃, CH₂Br₂ and CH₃I vs. CO₂ in Region 1 (a-c) and Region 2 (d-f). Type II major axis regression model (bivariate least squares regression) fits are shown for combined ORCAS and ATom-2 data, using data below 7 km for CHBr₃, CH₂Br₂, and below 2 km for CH₃I.

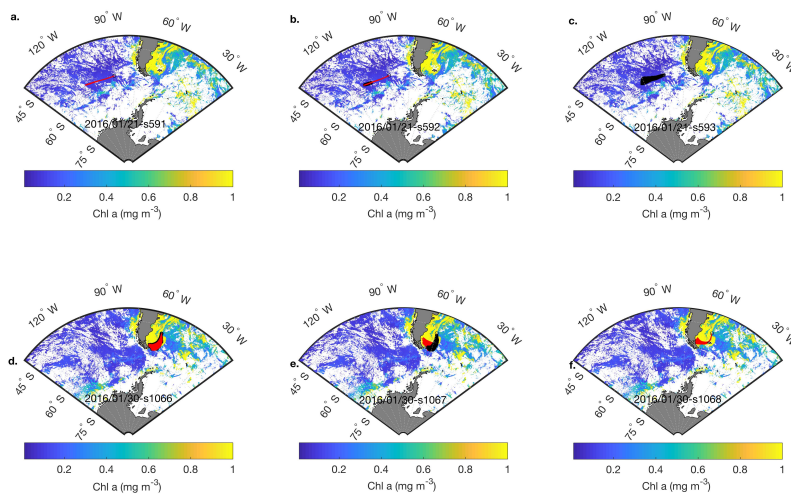


Figure S4. Two sets of three consecutive TOGA VOC sample locations, their back-trajectories and surface influences in the lower troposphere on two different flights (a-c; Jan. 21, 2016, and d-f; Jan. 30, 2016). For illustrative purposes, sampling locations are denoted by a black circle, 24-hour back trajectories are shown in red, and surface influences are shown with black squares in each subpanel, overlying weekly composites of remotely sensed chl *a*. Surface influence is multiplied by the underlying chl *a* (or other) surface field and averaged for each sample to yield a surface influence function.